



Engineering tunable dual peptide hybrid coatings promote osseointegration of implants

Zeyu Shou^{a,d,1}, Zhibiao Bai^{a,1}, Han Zhou^a, Yizhe Shen^a, Xiaojing Huang^a, Hongming Meng^a, Chenwei Xu^a, Shaohao Wu^a, Na Li^{d,**}, Chun Chen^{a,b,c,*}

^a Department of Orthopedics, The First Affiliated Hospital of Wenzhou Medical University, Wenzhou, 325000, People's Republic of China

^b Key Laboratory of Intelligent Treatment and Life Support for Critical Diseases of Zhejiang Province, Wenzhou, 325000, Zhejiang, People's Republic of China

^c Zhejiang Engineering Research Center for Hospital Emergency and Process Digitization, Wenzhou, Zhejiang, 325000, People's Republic of China

^d Wenzhou Institute, University of Chinese Academy of Sciences, Wenzhou, 325001, People's Republic of China

ARTICLE INFO

Keywords:

Implants
Osseointegration
Metal-phenolic networks
Block peptides
Surface modification

ABSTRACT

Utilizing complementary bioactive peptides is a promising surface engineering strategy for bone regeneration on osteogenesis. In this study, we designed block peptides, (Lysine)₆-capped RGD (K₆-(linker-RGD)₃) and OGP (K₆-linker-(YGFGG)₂), which were mildly grafted onto PC/Fe-MPNs through supramolecular interactions between K₆ and PC residues on the MPNs surface to form a dual peptide coating, named PC/Fe@K₆-RGD/OGP. The properties of the block peptides coating, including mechanics, hydrophilicity, chemical composition, etc., were detailedly characterized by various techniques (ellipsometry, quartz crystal microbalance, X-ray photoelectron spectroscopy, water contact angle, scanning electronic microscopy and atomic force microscopy). Importantly, the RGD/OGP ratio can be well adjusted, which allowed optimizing the RGD/OGP ratio to endow significantly enhanced osteogenic activity of MC3T3-E1 cells through the Wnt/β-catenin pathway, while also promoting cell adhesion, immune regulation, inhibiting osteoclast differentiation and oxidative stress reduction. In vivo, the optimized RGD/OGP coatings promoted bone regeneration and osseointegration around implants in rats with bone defects. In conclusion, rationally designed PC/Fe@K₆-RGD/OGP coating integrated RGD and OGP bioactivities, providing a convenient approach to enhance bioinert implant surfaces for bone regeneration.

1. Introduction

Successful osseointegration, defined as direct structural and functional integration between bone and implant, is critical for implant placement [1]. However, biological inertness of implants and challenging pathological conditions often lead to implant failure [2]. To optimize osseointegration, implant surface modifications that provide biological functions like enhanced biocompatibility, anti-inflammation, antioxidation, osteogenesis promotion, and osteoclast inhibition are promising strategies [3,4]. Various functional materials, including calcium phosphates [5,6] (hydroxyapatite and dicalcium phosphate) and bioactive molecules [7,8] (collagen, bone morphogenetic proteins, DNA, growth factors, and peptides), have been developed as implant coatings. Among these, bioactive peptides have attracted significant interest due to their excellent biocompatibility, stability and functional selectivity

[9].

Bioactive peptides can confer new functions to materials and modulate cell-material interactions [10]. With efficient and cost-effective peptide synthesis technology, the selection of peptide libraries has been expanded, and single peptides have shown certain effectiveness in tissue engineering applications. For example, cell-adhesion peptides (arginine-glycine-aspartic acid, RGD) derived from extracellular matrix (ECM) proteins have been used to modify the surfaces of a variety of materials to make them bioactive [11]. Osteogenic growth peptide (OGP) is a 14-amino acid polypeptide endogenous to human serum. The C-terminal fragment (YGFGG) has been identified as the active portion capable of enhancing osteoblast proliferation and differentiation, and has been widely used in bone tissue engineering [12]. Additionally, OGP-modified bone implants have demonstrated positive immunoregulation within the bone environment [13]. Other peptides, bone morphogenetic protein-2 (BMP-2) bioactive domain as

* Corresponding author. Wenzhou Institute, University of Chinese Academy of Sciences, Wenzhou, 325001, People's Republic of China.

** Corresponding author.

E-mail addresses: lina0701@ucas.ac.cn (N. Li), chenchunkk@163.com (C. Chen).

¹ These authors contributed equally to this work and are the first co-authors.

Abbreviations used

RGD	<i>arginine-glycine-aspartic</i>	ALP	<i>alkaline phosphatase</i>
ECM	<i>extracellular matrix</i>	TRAP	<i>tartrate-resistant acid phosphatase</i>
OGP	<i>osteogenic growth peptide</i>	CTSK	<i>cathepsin K</i>
BMP-2	<i>bone morphogenetic protein-2</i>	Col-1	<i>type I collagen</i>
VEGF	<i>vascular endothelial growth factor</i>	OPN	<i>osteopontin</i>
MPNs	<i>metal polyphenol networks</i>	OCN	<i>osteocalcin</i>
K ₆ -RGD	<i>K₆-(linker-RGD)₃</i>	ON	<i>osteonectin</i>
K ₆ -OGP	<i>K₆-linker-(YGFGG)₂</i>	qRT-PCR	<i>quantitative real-time polymerase chain reaction</i>
PC	<i>Proanthocyanidins</i>	IL-6	<i>interleukin 6</i>
FBS	<i>fetal bovine serum</i>	IL-10	<i>interleukin 10</i>
DMEM	<i>Dulbecco's modified Eagle's medium</i>	IFN- γ	<i>interferon-γ</i>
MEM	<i>Minimum Essential Medium Eagle</i>	LPS	<i>lipopolysaccharides</i>
QCM-D	<i>quartz crystal microbalance</i>	TNF- α	<i>tumor Necrosis Factor-α</i>
SEM	<i>scanning electron microscopy</i>	micro-CT	<i>micro-computed tomography</i>
WCA	<i>water contact angles</i>	BV	<i>bone volume</i>
AFM	<i>atomic force microscopy</i>	TV	<i>total volume</i>
		Tb-N	<i>trabecular number</i>
		BIC	<i>bone-implant contact</i>

an osteo-inductive growth factor induces bone morphogenesis [14]. Vascular endothelial growth factor (VEGF) mimetic peptides enhance endothelial cell migration and angiogenesis [15]. Antimicrobial peptides provide broad bactericidal effects for implant coatings [16]. However, due to the complexity of the challenging conditions faced in vivo applications, the effectiveness of single-function surface modification strategies is suboptimal, so researchers have started focusing on achieving multi-functional surface modification at the material interface [17].

Exploring combinations of complementary bioactive peptides has emerged as a promising strategy to confer versatility to the surface of implants. For instance, Sun et al. co-grafted RGD and BMP-2 peptides on Ti coatings, demonstrating a synergistic improvement in osteogenic capacity over individual peptides [18]. Geng et al. immobilized antimicrobial peptides (AMPs) and OGP on PEEK to achieve excellent host defense and tissue repair in bacterially contaminated bone defects [19]. Most recently, Liu et al. also utilized RGD and OGP peptides to construct a multifunctional coating with osseointegration in animal models [20]. Overall, biomimetic multi-peptide coatings have exhibited bioactivities exceeding individual peptides, with varied peptide ratios conferring distinct biological effects. However, precisely controlling spatial organization and dipeptide proportions through immobilization remains challenging. Various grafting methods, such as physical adsorption, coordination and covalent grafting, have been proposed for peptide coating construction [21,22]. However, covalent grafting relies on complex chemical modifications of dopa [23] molecules and peptides [22], facing issues like maintaining biological function and complex synthesis/purification. Physical adsorption and coordination are simple and direct, but often lead to drug exfoliation from weak non-covalent bonds, unable to provide long-term bioactivity [24]. Layer-by-layer (LbL) assembly offers straightforward, versatile surface modification yet has laborious protocols, low efficiency, and can bury bioactive molecules, preventing receptor detection [25]. Therefore, effective peptide combinations and immobilization techniques for maximized effects warrant further research.

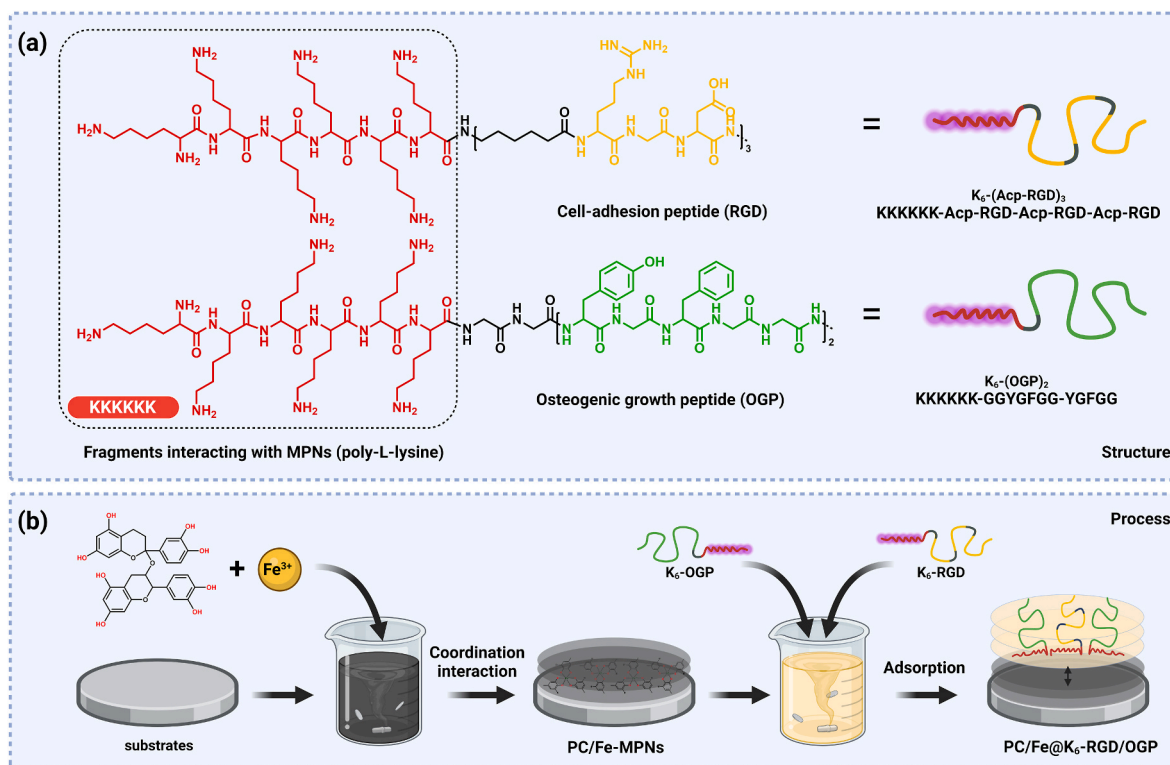
Polyphenols possess diverse bioactivities including anti-inflammatory, anticancer, antibacterial, and antioxidant effects [26]. In recent years, the metal polyphenol networks (MPNs) constructed by the coordination of metal ions and phenolic ligands [27] have received more and more attention due to its ability to deposit onto on various substrates and particles [28]. Although MPNs exhibit broad applicability of metal ions and polyphenol species, their capabilities still fall short in providing the functions are required throughout the complex processes of bone defect repair [29]. Physical or chemical immobilizing the

bioactive molecules onto the MPNs is the popular ways to change the biological destiny of MPNs. Polyphenols can interact with proteins through both covalent (Michael addition or Schiff base reaction) and noncovalent (hydrogen bonding, electrostatic interactions, and hydrophobic interactions) interactions, enabling polyphenol-protein coatings via approaches like self-assembled monolayers or layer-by-layer assembly [30]. We hypothesized that the peptide can interact with polyphenols in MPNs more efficiently through a rational designed assemble unit, which endowing the functions of peptide to MPNs. To test this hypothesis, two block peptides with complementary biofunctions, (Lysine)₆-capped RGD (K₆-(linker-RGD)₃) and OGP (K₆-linker-(YGFGG)₂), were designed (Scheme 1a), in which the positively charged K₆ was considered as the assembly unit and the linked short functional peptides of RGD and OGP was used to promote osteogenic differentiation in vitro and osseointegration in vivo. Our data demonstrated the RGD/OGP ratio deposited onto MPNs can be well adjusted by this strategy, and the optimized RGD/OGP coatings efficiently promoted bone regeneration and osseointegration around implants in rats with bone defects.

2. Materials and methods

2.1. Materials

Proanthocyanidins (PC, MW = 594.52), iron (III) nitrate nonahydrate (Fe(NO₃)₃·9H₂O), anhydrous sodium acetate and tris(hydroxymethyl)-aminomethane(Tris)(≥99 %) were obtained from Macklin. K₆-(linker-RGD)₃ (K₆-RGD, MW = 2111.51) and K₆-linker-(YGFGG)₂ (K₆-OGP, MW = 1864.18) synthesized by Hangzhou All Peptide Biotechnology Co., Ltd (Scheme 1a). Cell culture reagents including fetal bovine serum (FBS), Dulbecco's modified Eagle's medium (DMEM) and Minimum Essential Medium Eagle (MEM) were from Gibco. Paraformaldehyde, Triton X-100, rhodamine phalloidin (phalloidin-TRITC), 4,6-Diamidino-2-phenylindole (DAPI), Cell Counting Kit-8 (CCK-8), the ROS assay kit and ferric reducing antioxidant capacity (FRAP) assay kit were purchased from Sigma, Dojindo Laboratories and Beyotime Institute of Biotechnology. Titanium (Ti) plates, Ti rods and round glass coverslips (14 mm diameter, NEST) were cleaned with piranha solution (70 % H₂SO₄ and 30 % H₂O₂, V/V) at 98 °C for 2 h, followed by rinsing with Milli-Q water, and drying in a mild air stream before use (Caution: Piranha solution is highly oxidizing and corrosive and should be prepared and used with extreme caution). Experiments utilized deionized (DI) water purified by a Milli-Q system to a resistivity of over 18.25 M Ω cm.



Scheme 1. (a) Structure of the newly designed block peptide and (b) the main process of PC/Fe@ $K_6\text{-RGD/OGP}$ construction. Created with BioRender.com.

2.2. Preparation of PC/Fe@ $K_6\text{-RGD/OGP}$

A two-step aqueous room temperature synthesis was utilized to fabricate a PC/Fe@ $K_6\text{-RGD/OGP}$ hybrid coating composed of a PC/Fe-MPNs underlayer and $K_6\text{-RGD/OGP}$ peptide top layer (Scheme 1b).

PC/Fe-MPNs coatings were fabricated on $1\text{ cm} \times 1\text{ cm}$ substrates as previously reported [28]. To prevent further oxidation, the coating was immediately immersed in a PC solution before proceeding to the next step. $K_6\text{-RGD}$ and/or $K_6\text{-OGP}$ peptides (1 mg/mL) were dissolved in Tris-HCl buffer (10 mM, pH 7.5) to form peptide solutions. And by mixing $K_6\text{-RGD}$ and $K_6\text{-OGP}$ peptide solutions in different volume ratios (4:0, 3:1, 2:2, 1:3, 0:4), mixed peptide solutions with different feeding ratios were obtained. PC/Fe-MPNs coated substrates (1 cm^2 , 5 layers) were washed with DI water and blow-dried, then immersed in mixed peptide solution and incubated for 24 h to fabricate PC/Fe@ $K_6\text{-RGD/OGP}$ coatings with different feed ratios. Coated substrates were then rinsed with DI water and dried with gently air to obtain stable coatings.

2.3. Characterization

All prepared coatings were stored at $4\text{ }^\circ\text{C}$ and dried thoroughly prior to characterization. The thickness of silicon wafer-coated samples was determined by optical ellipsometry (M-2000UI, J.A. Woollam). The kinetic changes during the assembly of PC/Fe@ $K_6\text{-RGD/OGP}$ coatings on the chip surface were detected by a quartz crystal microbalance (QCM-D) with dissipation. The surface morphology of the silicon wafer-coated samples was examined by scanning electron microscopy (SEM) (SU8010, Hitachi). X-ray photoelectron spectra of silicon wafer-coated samples were obtained using a Thermo-Electron ESCALAB 250 spectrometer with a monochromatic Al source (1486.6 eV). The water contact angles (WCA) of the Ti plate surface were measured by static sessile drop method on a KRUSS DSA1 v1.80 analyzer. Zeta potentials of PC/Fe-MPN and PC/Fe@ $K_6\text{-RGD/OGP}$ coatings on polystyrene beads ($\varnothing = 3\text{ }\mu\text{m}$) were determined by Zetasizer Nano ZS ZEN3600 (WM2016002, Malvern).

2.3.1. Mechanical properties and surface morphology of coatings

Surface morphology, adhesion energy and roughness of coatings in liquid phase and in gas phase were characterized by atomic force microscopy (AFM) using a Dimension Icon system (Bruker). Samples were immobilized on AFM stages by vacuum adsorption. Silicon cantilever taps (MikroMasch NSCs/CSCs) were used to probe coating surfaces in percussion mode. Subsidiary software analyzed surface roughness from topographical maps. Young's moduli were derived by fitting retract curve force-separation data to the Derjaguin-Muller-Toporov (DMT) model.

2.3.2. Quantification of peptides adsorbed on the coating

To visualize the spatial distribution of polypeptide adsorption, blue fluorescently labeled RGD(MCA- $K_6\text{-RGD}$) and red fluorescently labeled OGP (TAMRA- $K_6\text{-OGP}$) block peptides were prepared. Different RGD:OGP volume ratios (4:0, 3:1, 2:2, 1:3, 0:4) were mixed and adsorbed on (PC/Fe)₅-MPNs coated substrates per the PC/Fe@ $K_6\text{-RGD/OGP}$ assembly method. Fluorescence changes pre- and post-assembly were monitored by laser scanning confocal microscopy (LSCM) (Nikon A1, Japan) to present Peptide distribution.

To quantify the mass of peptides adsorbed per unit area of the coating. The UV absorption spectra of the two labeled peptides were measured by a multimode microplate reader (Varioskan LUX, Thermo Scientific), and their respective standard curves at maximum absorbance were plotted. Then, the UV absorbance of the remaining labeled peptides in the solution before and after assembly of each ratio was measured and the amount and proportion of peptides were quantified by the standard curve. It is worth noting that the absorbance value of residual TAMRA- $K_6\text{-OGP}$ at 325 nm needs to be subtracted from the calculation of residual MCA- $K_6\text{-RGD}$ concentration. Finally, the concentration and proportion of peptides in PC/Fe@ $K_6\text{-RGD/OGP}$ coatings are calculated indirectly according to the feeding concentration.

2.3.3. Stability of PC/Fe@ $K_6\text{-RGD/OGP}$ in vitro and in vivo

In vitro stability of PC/Fe@ $K_6\text{-RGD/OGP}$ coatings was evaluated by

immersing samples in PBS (pH 7.3), 0.9 % NaCl and DMEM for 0–21 days, and the residual thickness measured by optical ellipsometry after rinsing and drying. To evaluate *in vivo* stability, PC/Fe@K₆-RGD/OGP-coated Ti rods were implanted into femoral defects of rats for 4 and 8 weeks, and the integrity of the surface coating was analyzed by SEM after gentle removal.

2.4. Cell culture

The Pre-osteoblasts MC3T3-E1 were purchased from ATCC and cultured with MEM medium (Gibco, 2276722, Waltham, USA) supplemented with 100U/ml penicillin, 100 mg/mL streptomycin and 10 % FBS. The Mouse bone marrow macrophages (mBMMs) were purchased from Pricella (CP-M141, Wuhan, China) and cultured with DMEM medium (Gibco, 2276722, Waltham, USA) supplemented with 100U/ml penicillin, 100 mg/mL streptomycin and 10 % FBS. Both cells keep in 75 mL Cell Culture Bottle at 37 °C and 5 % CO₂. The medium was replaced every 2–3 days. The cells were passaged using 0.25 % trypsin after reaching 90 % confluence.

2.4.1. Cell viability and proliferation assays

All prepared coatings were stored at 4 °C and thoroughly sterilized using high-pressure-steam Sterilization before *in vitro* and *in vivo* experiments. MC3T3-E1 were seeded onto 24-well plates coated with different coatings at a density of 1×10^4 cells per well. At 1-, 3- and 7-days post-seeding, cell viability was quantified using Cell Counting Kit-8 (CCK-8) assay. Briefly, culture medium was replaced with 350 μ L of basal medium plus 35 μ L of CCK-8 solution and incubated for 2 h at 37 °C. Afterward, the medium was transferred to 96-well plates and absorbance was measured at 450 nm using an Infinite 200 Pro microplate reader (Tecan, USA). In parallel samples at 3 days, the cytoskeletal and nuclei of MC3T3-E1 were fluorescently stained with rhodamine-phalloidin (red) and DAPI (blue), then imaged by LSCM to visually confirm cell adhesion and proliferation across the various substrates.

2.4.2. Cell migration test

When the cells had reached approximately 80 % confluence on the coatings, equal width scratches were made on the cell monolayer using a sterile 200 μ L pipette tip. The scratched areas were gently washed three times with phosphate-buffered saline (PBS). Medium without FBS was then added and the plates were cultured at 37 °C for 24 h. Microscopic images of the scratches were taken at 0 and 24 h using a microscope and analyzed using ImageJ software. Each experiment was repeated independently at least three times. The cell migration rate was calculated using the following formula:

$$\text{cell migration (\%)} = \left(1 - \frac{\text{width of the scratch at 24 h}}{\text{initial scratch width}} \right) * 100\%$$

2.4.3. Cell attachment and spreading at early stage

MC3T3-E1 were cultured on the coatings at a seeding density of 4×10^4 cells/cm². At 2 and 4 h after seeding, the cells were gently rinsed with PBS and then fixed with 4 % paraformaldehyde. 0.2 % Triton X-100 in PBS was used to permeabilize the cell membrane. F-actin filaments and nuclei were fluorescently labeled by staining with phalloidin-TRITC (red) and DAPI (blue). LSCM was used to visualize and assess cell morphology and cytoskeletal organization at these very early time points on the different substrates.

2.4.4. Intracellular ROS level and fluorescence analysis

Cells were seeded at 5×10^4 cells/cm² on glass coverslips and coatings. After 24 h, the complete medium was replaced with medium with or without 500 μ M H₂O₂ for 12 h to induce oxidative stress. To detect ROS levels, 2',7'-dichlorofluorescein diacetate (DCFH-DA, Beyotime, China, S0033) was diluted in serum-free medium to a final concentration of 10 μ mol/L. The fluorescence intensity of the DCFH-DA

probe was photographed by LSCM to visually examine the spatial localization of ROS generation within cells.

2.4.5. Osteogenic differentiation analysis

MEM medium containing 100U/ml penicillin, 100 mg/mL streptomycin and 10 % FBS was supplemented with 10 mM β -glycerol phosphate (Sigma-Aldrich, USA), 0.1 μ M dexamethasone (Sigma-Aldrich, USA), and 0.25 mM ascorbic acid (Sigma-Aldrich, USA) to prepare osteogenic medium. To induce osteogenic differentiation of BMSCs into osteocytes, BMSCs were co-cultured for several days with osteogenic induction medium.

Alkaline phosphatase (ALP) activity and alizarin red S (ARS) staining were used as early and late markers of osteogenic differentiation, respectively. MC3T3-E1 cells were seeded at a density of 2×10^4 cells/well. After 14 days of osteogenic induction, ALP activity was evaluated staining using the BCIP/NBT Alkaline Phosphatase Color Development Kit (Beyotime, China) and ALP Assay Kit (Beyotime, China) according to the manufacturer's instructions. To assess late-stage mineralization, cells were fixed with 4 % paraformaldehyde after 21 days of culture, then incubated with 0.1 % alizarin red S solution (pH 4.2) for 30 min. After observing and photographing with a microscope, calcium deposits were extracted using 10 % cetylpyridinium chloride solution for 1 h and quantified by measuring absorbance at 593 nm.

2.4.6. Osteoclast differentiation analysis

2.4.6.1. TRAP activity assay. DMEM medium containing 100U/ml penicillin, 100 mg/mL streptomycin and 10 % FBS was supplemented with 50 ng/mL Receptor Activator of Nuclear Kappa-B (RANKL) (Peprotech, USA) and 30 ng/mL Macrophage Colony-Stimulating Factor (M-CSF) (Peprotech, USA) to prepare osteoclast induction medium. To induce osteoclast differentiation, mBMMs were cultured with osteoclast induction medium for 5 days.

Tartrate-resistant acid phosphatase (TRAP) enzymatic activity in the conditioned media was assayed using a commercial kit (TRAP Assay Kit, Beyotime, China) according to the manufacturer's protocol. Briefly, sample was combined with acid phosphatase buffer incubated at 37 °C for 60 min. The reaction was stopped by addition of 0.5 N sodium hydroxide. Absorbance was measured at 405 nm using a microplate reader to quantify the generation of pNP from the substrate. TRAP activity was expressed as micromolar pNP produced per minute per milligram of total cellular protein.

2.4.6.2. Actin and TRAP staining of osteoclasts. mBMMs cells were cultured on different coatings and treated with 50 ng/mL RANKL and 30 ng/mL M-CSF for 5 days to induce differentiation. Cells were fixed in 4 % paraformaldehyde for 15 min and permeabilized with 0.1 % Triton X-100 for 5 min. Actin cytoskeleton organization was examined by phalloidin-TRITC staining followed by nuclear staining with DAPI. Multinucleated cells containing ≥ 3 nuclei were classified as mature osteoclasts. Additionally, osteoclast formation was evaluated by TRAP staining. Fixed cells were incubated with TRAP solution (Sigma-Aldrich) for 30 min at room temperature and imaged using brightfield microscopy. TRAP-positive multinucleated cells and F-actin ring areas were quantified by automated analysis using ImageJ software.

2.4.7. Gene expression detected by RT-qPCR

To further study the influence of these coatings on the osteogenesis of MC3T3-E1 cells, osteogenesis-related genes, including β -catenin, type I collagen (Col-1), osteopontin (OPN), osteocalcin (OCN), and osteonectin (ON) were investigated using quantitative real-time polymerase chain reaction (qRT-PCR). After co-culture with these coatings for 7 days in osteogenic induction medium, total RNA from cultured cells was extracted using TRIzol Reagent. To silence the expression of β -catenin, MC3T3-E1 were pretreated with β -catenin-siRNA before being cultured

with these materials, with those treated with nontargeting siRNA (NVC) as the control group. The concentration and purity of the extracted RNA were determined by measuring the absorbance at 260 and 280 nm (BioTek, USA). Afterward, an equivalent amount of RNA was processed to generate cDNA using HiScript III All-in-one RT SuperMix Perfect for qPCR kits (Vazyme, China). After reverse transcription, the qRT-PCR experiment was performed using a Real-Time PCR system (Light-Cycler480, Roche, USA). The relative expression of the target gene was normalized against the housekeeping gene β -Actin. The results were analyzed using the $2^{-\Delta\Delta CT}$ method. On the other hand, the mRNA expression levels of inflammatory factors (interleukin 6 (IL-6) and interleukin 10 (IL-10)) and osteoclastogenesis-related markers (including cathepsin K (CTSK), tartrate resistant acid phosphatase (TRAP)) were measured using qRT-PCR assay as mentioned above. The primer sequences for the selected genes are listed in Table S1.

2.5. Macrophage polarization *in vitro* and *in vivo*

mBMMs were seeded on the different modified Ti substrates and cultured under conditions that mimic a pro-inflammatory M1 environment containing 50 ng/mL lipopolysaccharides (LPS, Sigma, USA) and 50 ng/mL interferon- γ (IFN- γ , Peprotech, USA). After 24 h, the cells and supernatant were collected. First, fluorescence-activated cell sorting (FACS) was performed to detect the surface markers of polarized macrophages. The cells were incubated with fluorescein isothiocyanate (FITC)-conjugated anti-CD86 and allophycocyanin (APC)-conjugated anti-CD206 antibodies (Biolegend, USA) at 4 °C for 30 min to confirm the M1 (CD86⁺) and M2 (CD206⁺) phenotypes. The cells were analyzed using a flow cytometer (CytoFLEX, Beckman Coulter, USA), and the results were analyzed using the CytExpert software. In addition, the prepared supernatant was used to detect M1 (Tumor Necrosis Factor- α , TNF- α) and M2 (IL-10) macrophage cytokines using enzyme-linked immunosorbent assay (ELISA) kits (Multisciences, China) according to the manufacturer's instructions.

To study the regulatory effects on macrophage polarization, the Ti substrates were subcutaneously implanted into rats. At 5 days post-implantation, the samples were harvested and processed for immunofluorescence staining. Briefly, the samples were fixed, blocked, and incubated overnight at 4 °C with fluorescein isothiocyanate (FITC)-conjugated anti-iNOS and Cyanine 3 (Cy3)-conjugated anti-CD68 antibodies, and Alexa Fluor 647-conjugated anti-CD206 antibodies (M2 marker). After washing, the sheets were mounted with antifade medium containing DAPI, and imaged using LSCM. ImageJ was utilized to analyze the area occupied by double-positive cells.

2.6. Osteogenesis evaluation *in vivo*

Thirty Sprague Dawley (SD) rats (male, 6 weeks) weighing approximately 300 g were divided into five groups (n = 3): control (uncoated Ti rods), Ti-PC/Fe-MPNs (Ti rods coated with PC/Fe-MPNs), and Ti-PC/Fe@K₆-RGD/OGP (Ti rods coated with PC/Fe@K₆-RGD/OGP with different ratios). After intraperitoneal anesthesia with 10 % sodium pentobarbital (1 mL/100 g), a skin incision was made on the lateral side of the rat femur to expose the femur. The 1 mm diameter, 6 mm long implants were inserted perpendicularly into the femurs under constant cooling with 0.9 % NaCl solution. After disinfection with povidone iodine, the incision was sutured and cefuroxime sodium was administered intramuscularly daily for postoperative infection prophylaxis. After 5 and 8 weeks, rats were euthanized by overdose of sodium pentobarbital, and femur samples were collected. Samples were fixed in 4 % paraformaldehyde for further analysis. All animal experiments were performed according to the Animal Care Guidelines of the Wenzhou Institute, University of Chinese Academy of Sciences (WUCAS) and approved by the Animal Ethics Committee of WUCAS.

2.6.1. Microfocus computed tomography (Micro-CT)

The femurs containing the implants were scanned using a micro-computed tomography (micro-CT) scanner operated at 80 kV, 300 μ A, and 360° rotation with a 0.6° step. A region of interest (ROI) 200 μ m from the implant surface was reconstructed using associated CTAn and CTVol software. Bone volume (BV), total volume (TV), and trabecular number (Tb. N) were measured from the reconstructed three-dimensional images.

2.6.2. Histological analysis

Osteogenesis and osseointegration on the surfaces of Ti screws were evaluated through histological staining and quantitative analysis. The samples were first fixed with paraformaldehyde, washed with water, dehydrated with ethanol and clarified with xylene, before being embedded in poly (methyl methacrylate). Next, the embedded blocks were sliced into longitudinal sections measuring 300 μ m in thickness at the implantation center using a hard tissue slicer (EXAKT 300CP), and further ground down to 10 μ m thickness using a Grinding System (EXAKT 400 CS). Toluidine blue staining was then applied to the samples, and optical microscope images were taken using a Ni-U microscope from NIKON. Using Image-Pro Plus6.0 software, bone-implant contact (BIC) was quantified, representing the percentage of implant circumference directly in contact with bone tissue in the threaded area. The mean BIC (%) was determined using the following formula:

$$\text{mean BIC (\%)} = \left(\frac{\text{contact lengths between bone and implant}}{\text{length of the implant within the bone tissue}} \right) * 100\%$$

2.6.3. Biomechanical push-out test

The interfacial shear strength between bone and implant was assessed through push-out testing. Specifically, femur samples containing Ti rod implants were secured onto an Instron E10000 instrument, which was outfitted with a 500 N load cell. The Ti rods were then gradually pulled out from the surrounding bone at a constant rate of 1 mm/min, until complete detachment occurred. The interfacial shear strength was determined as the maximum load at implant failure and was recorded for further analysis.

2.7. Data processing and statistical analysis

Statistical analyses were performed using GraphPad Prism 9.5 (GraphPad Software Inc., CA, USA) and the graphical representation was done using Origin 2023b (OriginLab, MASS, USA). The results are expressed as mean \pm standard deviation (SD). The significance between the experimental groups was assessed using the *t*-test and indicated by the symbols “*”, “**”, and “***” for $p < 0.05$, $p < 0.01$ and $p < 0.001$, respectively. In addition, statistical significance compared to the Control group was marked by # $p < 0.05$, ## $p < 0.01$ or ### $p < 0.001$, while non-significant differences were labeled as “ns”. All experiments were independently replicated three times, unless otherwise specified.

3. Results and discussions

3.1. Characterization of the PC/Fe@K₆-RGD/OGP coating

The (PC/Fe)_n-MPNs coatings were fabricated following previous reports, exhibiting linear growth characteristics (Fig. S1) relative to the number of layers. The PC/Fe@K₆-RGD, PC/Fe@K₆-OGP, PC/Fe@K₆-RGD/OGP coatings were constructed by grafting K₆-RGD, K₆-OGP, K₆-RGD/OGP peptides onto (PC/Fe)₅-MPNs coatings (32.125 \pm 2.314 nm). Optimal graft thickness growth of different peptides was achieved by optimizing the grafted PH (Figs. S2a–c). Immersing (PC/Fe)₅-MPNs in 1 mg/mL RGD/OGP (1:1) at pH 7.5 for 24 h resulted in an appropriate thickness of PC/Fe@K₆-RGD/OGP coating of 40.80 nm (thickened by 8.917 \pm 1.436 nm) (Fig. 1a). QCM-D monitoring under pH 7.5 showed continuous deposition of K₆-RGD, K₆-OGP and K₆-RGD/OGP peptides

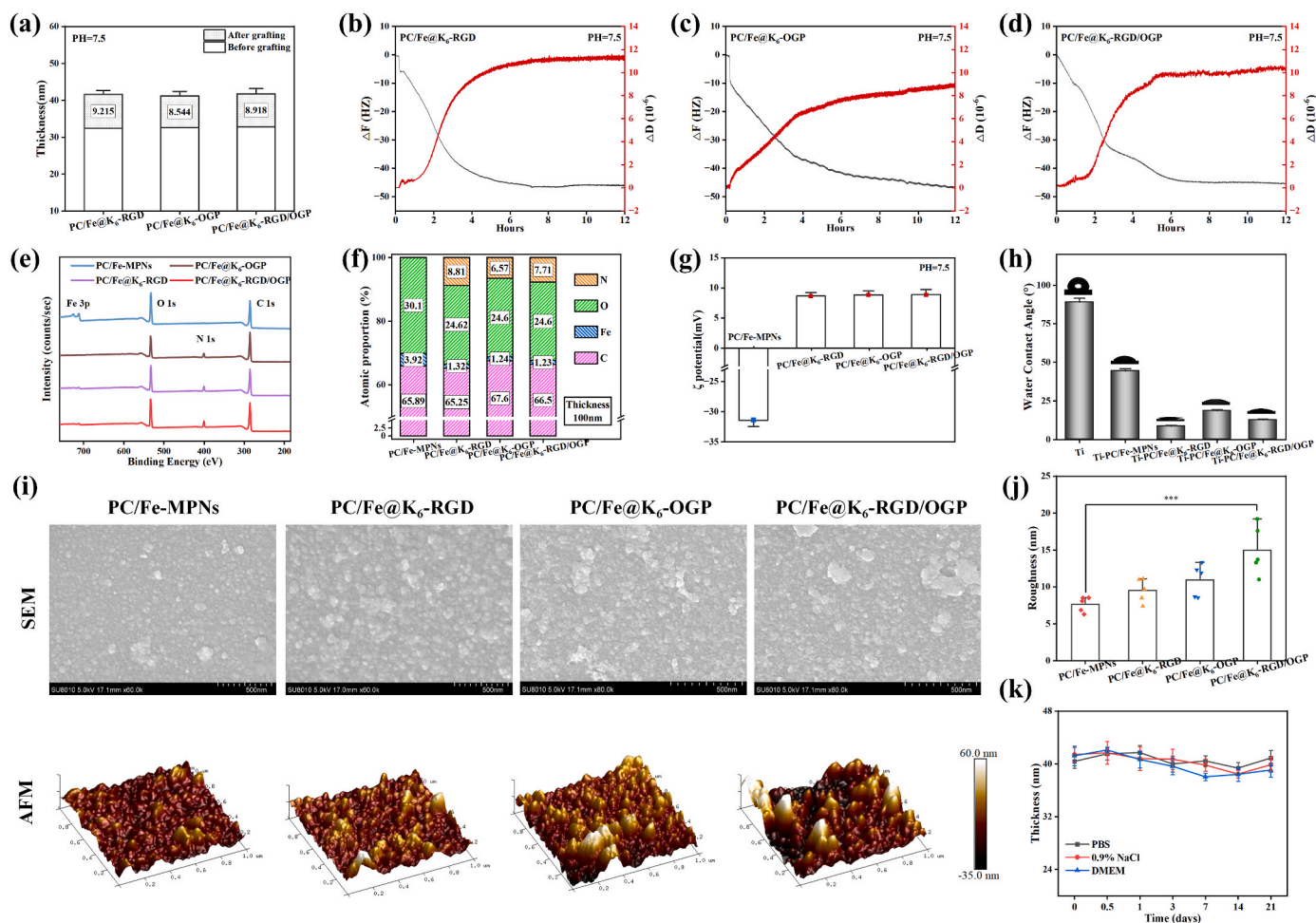


Fig. 1. Characterization of the PC/Fe@K₆-RGD/OGP coating. (a) Thickness growth of PC/Fe@K₆-RGD, PC/Fe@K₆-OGP, and PC/Fe@K₆-RGD/OGP at PH = 7.5. The shifts of ΔF and ΔD monitored by QCM-D during fabricating (b) PC/Fe@K₆-RGD, (c) PC/Fe@K₆-OGP and (d) PC/Fe@K₆-RGD/OGP coatings at pH 7.5. (e) Total XPS spectra and (f) the molar ratio of elements of PC/Fe@K₆-RGD, PC/Fe@K₆-OGP, and PC/Fe@K₆-RGD/OGP coatings. (g) Zeta potential changes of coating surface resulting from different peptides adsorption on (PC/Fe)₅-MPNs, while surface hydrophilicity changes of both types of composite coatings are shown in (h). (i) SEM and 3D AFM images of the front of PC/Fe@K₆-RGD, PC/Fe@K₆-OGP and PC/Fe@K₆-RGD/OGP coatings in air. (j) The roughness quantification of these coatings. (k) The change of coating thickness with treatment time in PBS, 0.9%NaCl, DEME. Scale bars in (i) are 500 nm. (N \geq 3, no significance noted as “ns”, *p < 0.05, **p < 0.01, ***p < 0.001 using *t*-test.)

during coating, indicated by decreasing ΔF and increasing ΔD (Fig. 1b–d). The thickness of peptides deposited on the surface of (PC/Fe)₅-MPNs in liquid phase was obtained by the Voigt model in the affiliated software of QCM-D and showed a trend of gradual increase with the addition time of peptides (Figs. S3a–c). QCM-D confirmed successful peptide grafting and revealed a mixed peptide layer of 9.59 nm. The elemental distribution of the coatings was investigated by XPS, which directly demonstrated the successful grafting of K₆-RGD, K₆-OGP and K₆-RGD/OGP peptides onto the PC/Fe-MPNs surface by the appearance of the N1s peak and the weakening of the Fe peak intensity (Fig. 1e). The grafting situation of the peptides on the coating surface was also reflected in the changes of the elemental ratios (Fig. 1f). Within the depth range that XPS can probe, we can calculate that the molar ratio of RGD to PC molecules in the PC/Fe@K₆-RGD coating was about 1: 5.15; the molar ratio of OGP to PC molecules in the PC/Fe@K₆-OGP coating was about 1: 5.3, respectively (Table S2).

Grafting of K₆-RGD, K₆-OGP and K₆-RGD/OGP peptides changed the surface charge and hydrophobicity of the coatings. Zeta potential changes of coatings coated on polystyrene (PS) beads were measured. The results in Fig. 1g show that the surface of (PC/Fe)₅-MPNs was negatively charged, while the surfaces of PC/Fe-MPNs coatings modified with K₆-conjugated peptides exhibited a significant increase in charge, which was due to the large number of lysine residues in K₆. The

hydrophobicity changes of the coatings deposited on Ti substrates were observed using a contact angle goniometer. As shown in Fig. 1h, the water contact angle (WCA) of peptide-grafted Ti surfaces were significantly lower than that of bare Ti surfaces. The exceptional hydrophilicity of peptides, particularly RGD peptides, accounts for this observation. SEM and AFM were used to observe the coatings at the nanoscale and found that PC/Fe-MPNs, PC/Fe@K₆-RGD, PC/Fe@K₆-OGP and PC/Fe@K₆-RGD/OGP were uniformly deposited on the Ti surface and formed a rough surface (Fig. 1i). Fig. 1j shows that the analyzed roughness of peptide-grafted PC/Fe-MPNs surfaces increased compared to PC/Fe-MPNs surfaces, among which PC/Fe@K₆-RGD/OGP had the highest roughness. As a composite coating with the potential to promote tissue integration and repair, it must remain stable under physiological conditions. The coatings were immersed in PBS, 0.9 % NaCl solution, DMEM medium, and the change in thickness over time was monitored (Fig. 1k). The results showed that the thickness of the coatings did not significantly decrease during the 21 days observation period, indicating that the PC/Fe@K₆-RGD/OGP composite coating remained stable under physiological conditions.

3.2. Mechanical properties of coatings

In an attempt to delve deeper into the mechanical properties of the

coating surfaces, AFM was used to investigate the structures and properties of various bioactive coatings in both gas and liquid phases. Similar to the gas phase, all coatings in the liquid phase exhibited discontinuous rough structures formed by the adhesion and aggregation of numerous particles (Fig. 2a). The roughness was fitted using the Nano Scope analysis software, and as shown in Fig. 2d, the PC/Fe@K₆-RGD/OGP coating in the liquid phase (6.976 ± 0.454 nm) showed a significant

change compared to the PC/Fe-MPNs (9.142 ± 0.431 nm). This value was noticeably higher than both PC/Fe@K₆-RGD (7.682 ± 0.500 nm) and PC/Fe@K₆-OGP (8.042 ± 0.561 nm). Fig. S4a and Fig. 2b illustrate the Young's modulus of the coatings in the liquid and gas phases along with their distribution curves. The quantitative analysis results in Fig. 2e reveal that the PC/Fe@K₆-RGD/OGP coating displayed a higher Young's modulus in the liquid phase (8.255 ± 0.301 MPa) compared to the PC/

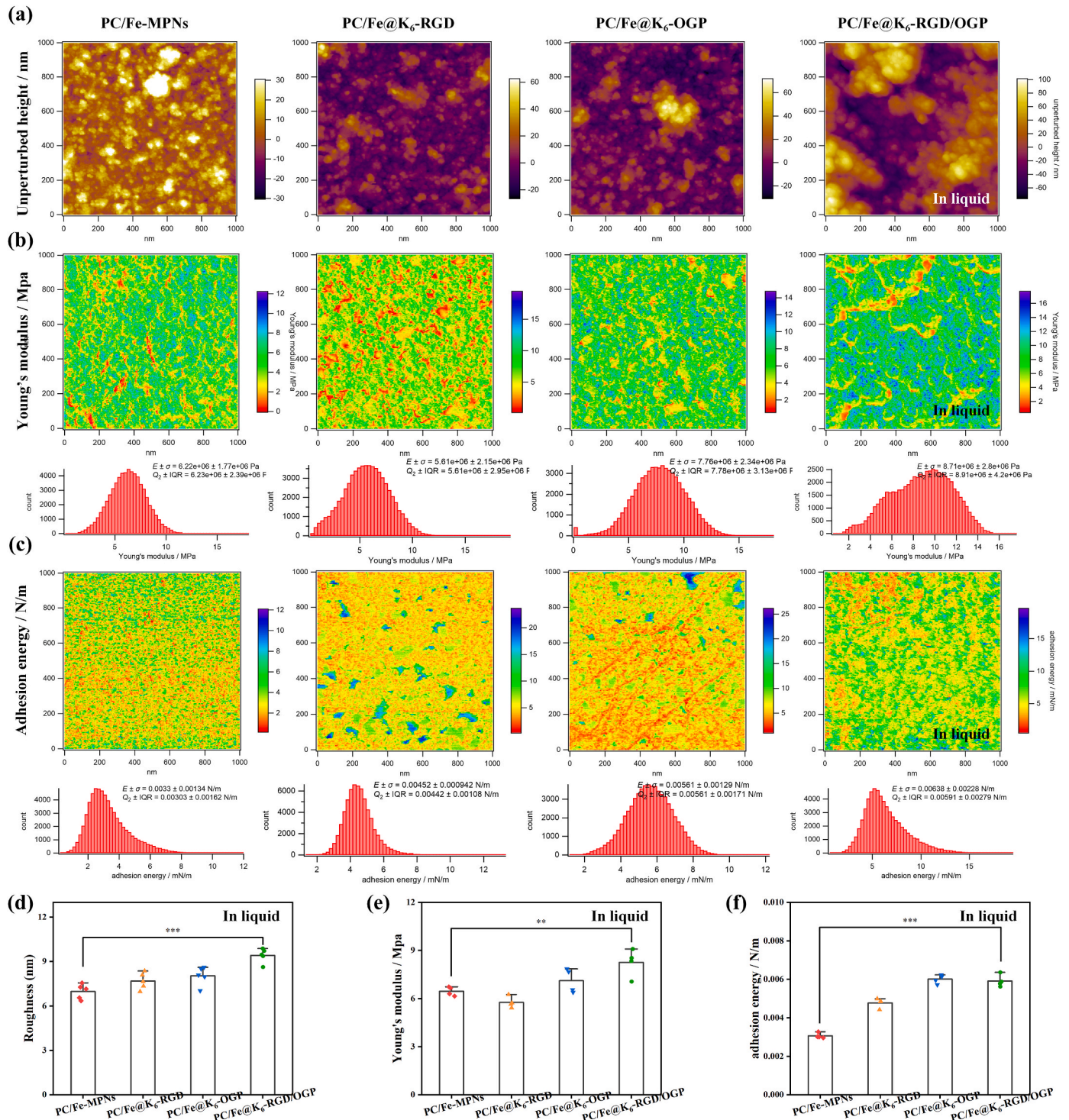


Fig. 2. Mechanical properties of different coatings. (a) AFM images of the front of PC/Fe-MPNs, PC/Fe@K₆-RGD, PC/Fe@K₆-OGP, and PC/Fe@K₆-RGD/OGP in liquid. (b) Young's modulus images and curves of PC/Fe-MPNs, PC/Fe@K₆-RGD, PC/Fe@K₆-OGP, and PC/Fe@K₆-RGD/OGP in liquid. (c) Adhesion energy images and curves of PC/Fe-MPNs, PC/Fe@K₆-RGD, PC/Fe@K₆-OGP, and PC/Fe@K₆-RGD/OGP in liquid. (d) The roughness, (e) young's modulus, and (f) adhesion energy quantification of these coatings in liquid. ($N \geq 3$, no significance noted as "ns", * $p < 0.05$, ** $p < 0.01$, *** $p < 0.001$ using t -test.)

Fe-MPNs coating (6.46 ± 0.242 MPa), and exceeded the PC/Fe@K₆-RGD (5.76 ± 0.305 nm) and PC/Fe@K₆-OGP (7.115 ± 0.651 nm). Fig. S4b presents a similar trend in the gas phase, indicating improved hardness and stiffness in two peptide-modified coating materials, leading to a superior resistance to external forces. Fig. S4c and Fig. 2c show the adhesion energies of the coatings and their mechanical curves. The results in Fig. 2f indicate that the PC/Fe@K₆-OGP (6.01 ± 0.196 mN/m) and PC/Fe@K₆-RGD/OGP (5.91 ± 0.276 mN/m) coatings have higher adhesion energies in the liquid phase compared to the PC/Fe-MPNs coating (3.065 ± 0.121 mN/m). Fig. S4d depicts a similar phenomenon in the gas phase. This suggests that the newly designed coatings can adhere more securely to the substrate and therefore have a longer life.

3.3. Quantification of peptides adsorbed on the coating

The above results proved the successful construction of PC/Fe@K₆-RGD/OGP composite coating, and various characterization results such as QCM-D indicated that the growth patterns of K₆-RGD and K₆-OGP on the PC/Fe-MPNs coating surface were similar. Therefore, it is worth exploring to determine whether the final ratio of K₆-RGD and K₆-OGP in PC/Fe@K₆-RGD/OGP composite coatings can be affected by changing the feeding ratio of K₆-RGD and K₆-OGP to affect their biological properties. Firstly, we used LSCM to observe the distribution of fluorescent peptides on the coated surface. As shown in Fig. 3a, a homogeneous fluorescence distribution was observed across the experimental groups, indicating the even distribution of peptides on the surfaces. On the surface of PC/Fe-MPNs treated solely with MCA-K₆-RGD peptide, red light was unobservable, while blue light was perceptible. In contrast, blue light was not detectable on pure Tamra-K₆-OGP peptide-treated PC/Fe-MPNs, but red light could be easily observed. Furthermore, in PC/Fe@K₆-RGD/OGP coating with different feeding ratios, the decrease in MCA-K₆-RGD incorporation resulted in a gradual decline in blue fluorescence intensity. Similarly, the quantity of Tamra-K₆-OGP peptide increased and the intensity of red fluorescence gradually augmented. The above phenomenon of blue or red fluorescence changing with the change of feed ratio possibly indicate the successful immobilization of K₆-RGD and K₆-OGP peptide at the predetermined ratios.

The trend of fluorescence intensity of the coating with respect to the feed ratio was further confirmed by quantitative results obtained through standard curve analysis of the UV absorbance of MAC-K₆-RGD

and TAMRA-K₆-OGP (Fig. S5). The result of Fig. 3b showed that the corresponding peptide densities in PC/Fe@K₆-RGD and PC/Fe@K₆-OGP were found to be 43.54 ± 2.93 and 37.01 ± 1.21 $\mu\text{g}/\text{cm}^2$, respectively. After treatment with an RGD: OGP solution of mass ratio 2:2, the concentration of immobilized K₆-RGD on the PC/Fe@K₆-RGD/OGP coating was 22.05 ± 1.44 $\mu\text{g}/\text{cm}^2$, while that of K₆-OGP was 19.01 ± 1.34 $\mu\text{g}/\text{cm}^2$. The molar ratio of immobilized K₆-RGD to K₆-OGP (1.02:1) on the PC/Fe@K₆-RGD/OGP coating was similar with the feeding ratio, and also not far from with the molar ratio of RGD to OGP peptides (0.95:1) calculated from the surface element distribution as shown in Fig. 1f and Table S2. Notably, immobilization ratio onto the PC/Fe@K₆-RGD/OGP coatings exhibited consistent variation across different feed ratios, namely with 3:1 or 1:3 solutions. Specifically, Fig. 1c illustrates the density ratio of grafted peptides on the coating surface changing proportionally with the feeding ratio of 3:1, 2:2, and 1:3.

3.4. Cell proliferation, anchoring and migration capacity on different coatings

Biomaterials, once implanted, can reside within the body for short-term, long-term, or even permanent durations. The cellular activity at the interface of the implant primarily determines the success of osseointegration [31]. To enhance the cytocompatibility of the coating, we designed the PC/Fe@K₆-RGD/OGP coating. By regulating the feeding ratio of the two synergistic peptides, we aimed to construct a more efficiently bioactive interface.

We assessed the capability of MC3T3-E1 cells to colonize, proliferate, survive and migrate on all coating surfaces. After 3 days of culture, cells seeded on all coating surfaces were stained with DAPI (nucleus, blue) and TRITC Phalloidin (cytoskeleton, red) (Fig. 4a). Cells adapted well to all surfaces regardless of coating types, demonstrating excellent cytocompatibility of all coating surfaces. Cell viability on days 1, 3 and 7 was quantified using the CCK-8 assay (Fig. 4b). Peptide-modified coating surfaces supported significantly higher cell numbers and vitality compared to PC/Fe-MPNs and Ti surfaces. Notably, surfaces modified with both peptides exhibited distinctly enhanced cell viability compared to individual peptide modified PC/Fe@K₆-RGD and PC/Fe@K₆-OGP coatings. For the early cell anchoring experiments of MC3T3-E1 cells, serum-free media were used to evaluate the initial adhesion of MC3T3-E1 cells onto diverse substrates, given the inevitable impact of serum

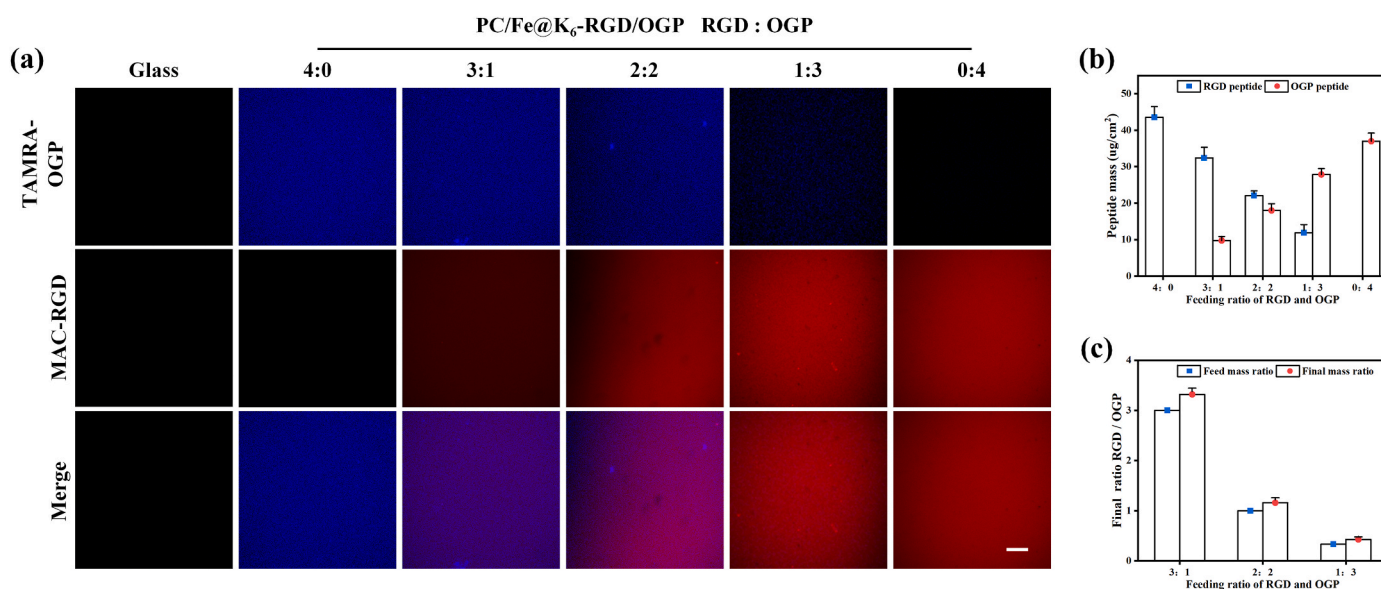


Fig. 3. (a) Visualization of fluorescently labeled peptides (TAMRA-K₆-OGP peptide and MCA-K₆-RGD peptide) immobilized on PC/Fe-MPNs coating. (b) The peptide density of PC/Fe@K₆-RGD/OGP coating with different feeding ratios indirect calculated from the standard curve. (c) Comparison of final ratio and feed ratio of two peptides in PC/Fe@K₆-RGD/OGP coating. Scale bars in (a) are 50 μm ($N \geq 3$).

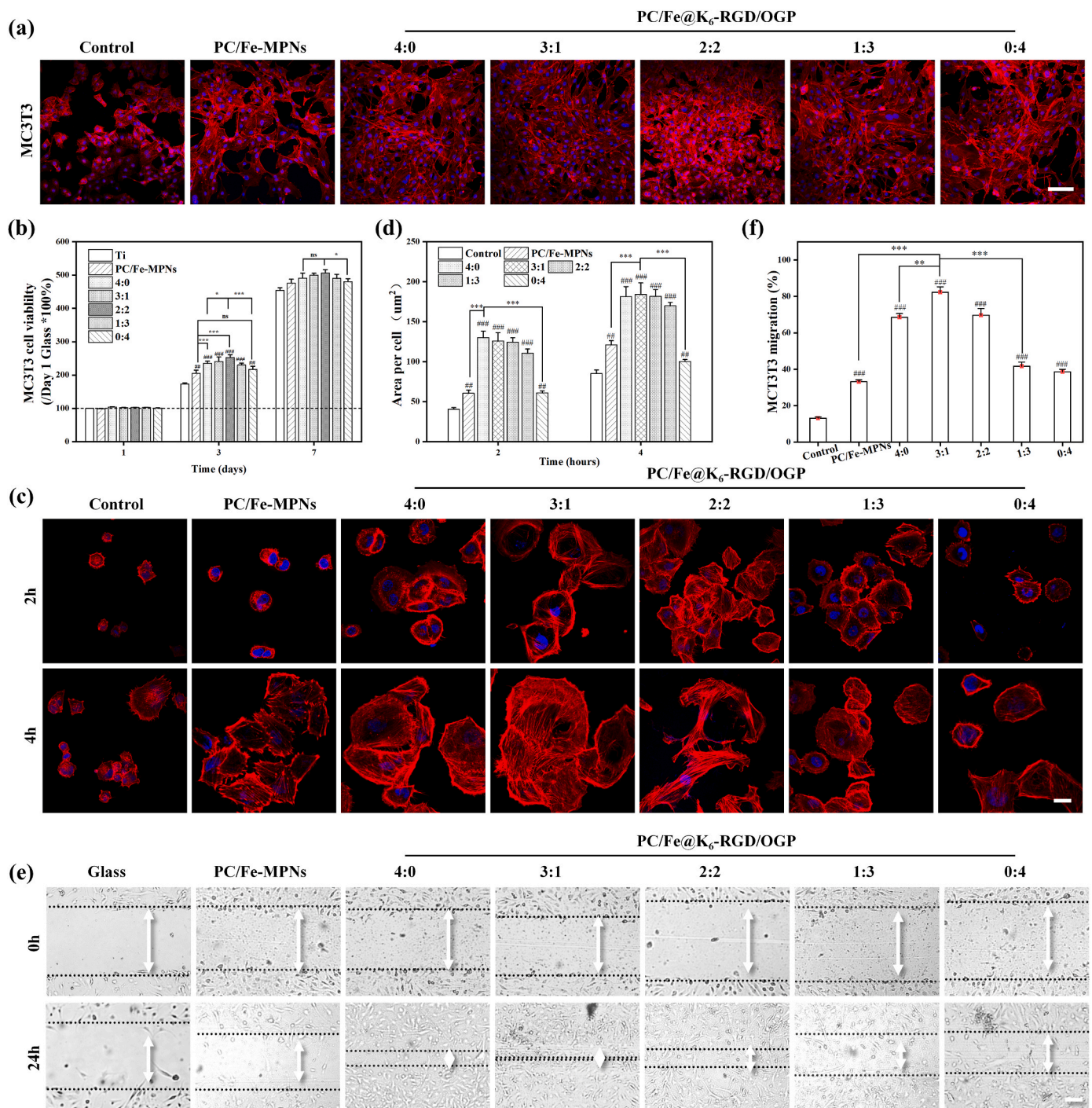


Fig. 4. Cell proliferation, anchoring and migration capacity of different coated modified substrates. **(a)** Representative images of cytoskeleton staining after 3 days of culture on different coatings. **(b)** Comparison of MC3T3-E1 cell viability on days 1, 2, and 3. **(c)** Fluorescence microscopy images of MC3T3-E1 cells seeded on different coatings for 2 and 4 h. **(d)** Area per cell of the seeded MC3T3-E1 of (c). **(e)** Representative images of MC3T3-E1 cells migration after 24 h of culture on different coatings. **(f)** Comparison of cell mobility in (e). Scale bars in (a) are 100 μm, scale bars in (c) are 50 μm, scale bars in (e) are 200 μm. (N ≥ 3, no significance noted as “ns”, *p < 0.05, **p < 0.01, ***p < 0.001 using *t*-test, and #p < 0.05, ##p < 0.01 or ###p < 0.001 compared with the Control group.)

constituents on non-specific cellular adhesion. After 2 h and 4 h of incubation, adherent MC3T3-E1 cells were detected via TRITC Phalloidin staining (Fig. 4c), and single cell areas were statistically analyzed using ImageJ (Fig. 4d). As expected, under serum-free conditions, while cells adhered to all substrata, coatings containing RGD peptide, namely PC/Fe@K₆-RGD, PC/Fe@K₆-RGD/OGP (3:1) and PC/Fe@K₆-RGD/OGP (2:2), demonstrated earlier and clearer cell adhesive capability compared to the control group and PC/Fe-MPNs surface. To validate the impact of coatings on cell migratory ability, scratches were made on peptide-

modified coating surfaces with adhered cells (without damaging the coatings), and cell migration was observed microscopically after 24 h incubation in serum-free media (Fig. 4e), with migration rates calculated (Fig. 4f). As expected, cells on the control group and PC/Fe-MPNs surfaces exhibited little migration, whereas distinctly enhanced migratory abilities were observed on peptide-modified PC/Fe-MPNs surfaces, especially on PC/Fe@K₆-RGD/OGP (3:1) coating.

The results suggest that the PC/Fe@K₆-RGD/OGP coating with co-immobilized RGD and OGP peptides demonstrates a more potent

effect in promoting MC3T3-E1 cell adhesion, migration and proliferation. This is attributed to the specific binding of RGD peptides to integrin receptors (e.g., $\alpha v\beta 3$, $\alpha 5\beta 1$) on the cell membrane, thereby activating downstream signaling pathways including protein kinase C, MAPK and tyrosine kinases. Concurrently, the immobilized OGP peptides can effectively stimulate osteoblastic proliferation and metabolism. By optimizing the ratios of RGD and OGP peptides within the coating, their synergistic effects can enhance MC3T3-E1 cellular adhesion, migration and proliferation, which are critical for early osteogenesis and

osseointegration in vivo.

3.5. Osteogenic differentiation of MC3T3-E1 on different modified substrates

The balance between osteoblasts and osteoclasts is closely related to the bone healing mechanism, and higher osteogenic activity of osteoblasts favors bone formation over osteoclastic differentiation, thereby integrating implants into bone through new bone formation [32,33]. We

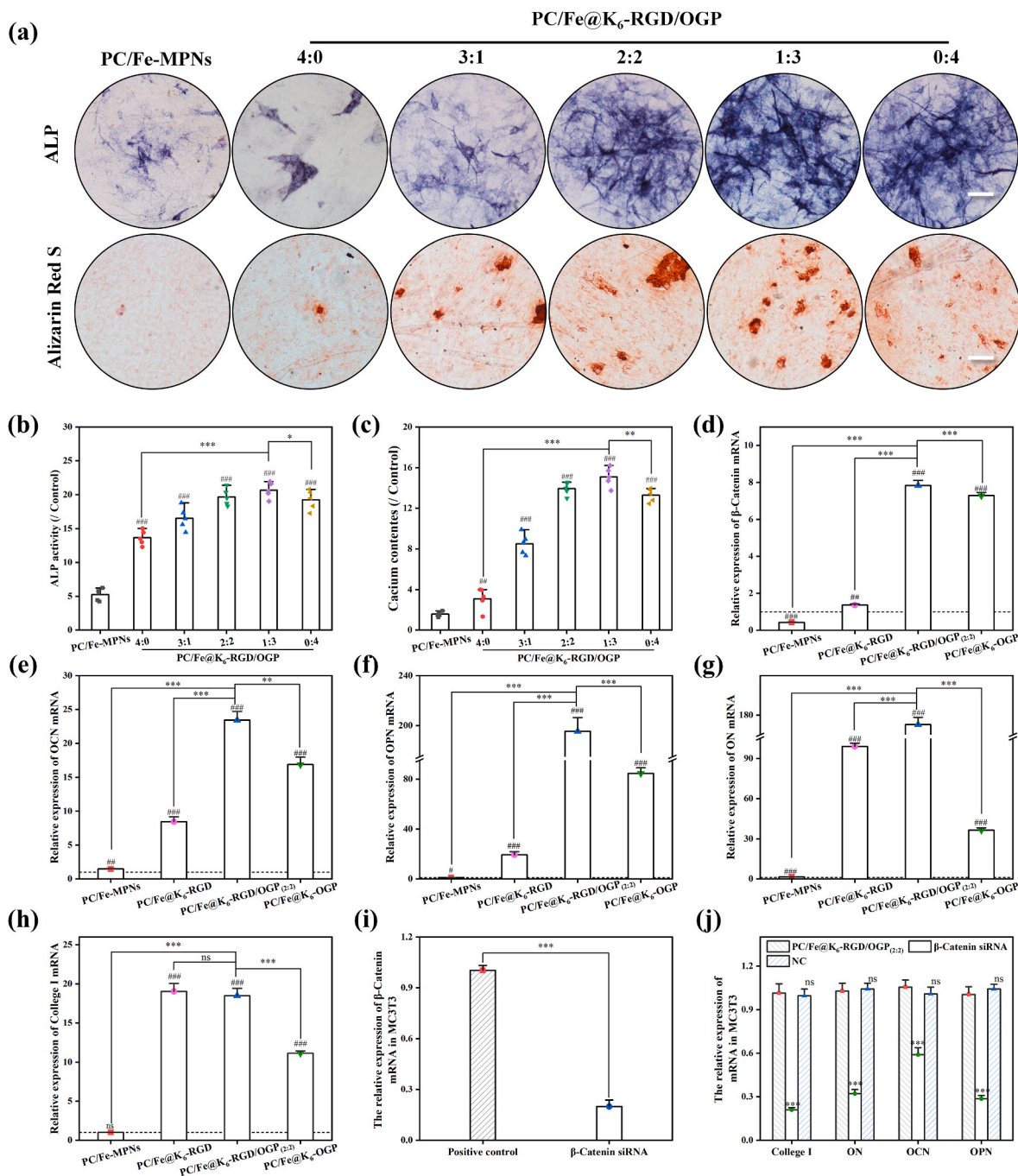


Fig. 5. Osteodifferentiation of MC3T3-E1 on different modified substrates. (a) Representative images of ALP staining after 7 days of co-culture with PC/Fe@K₆-RGD/OGP and Alizarin Red S staining after 21 days. (b) Quantitative analysis of ALP activity. (c) Quantitative analysis of calcium deposition. Relative mRNA expression of (d) β -Catenin, (e) OCN, (f) OPN, (g) ON and (h) College I genes in MC3T3-E1 cultured in different modified substrates for 7 days. (i) The mRNA level of β -catenin in MC3T3-E1 pretreated by corresponding siRNA, with NC siRNA as control. (j) Pretreatment of siRNA targeting β -catenin effectively inhibit the up-regulation of OCN, OPN, ON, on and College I in MC3T3-E1 induced by PC/Fe@K₆-(RGD/OGP)_{2:2}. Scale bars in (a) are 100 μ m, scale bars in (b) are 200 μ m.. (N \geq 3, no significance noted as “ns”, *p < 0.05, **p < 0.01, ***p < 0.001 using t-test, and #p < 0.05, ##p < 0.01 or ###p < 0.001 compared with the Control group.). (For interpretation of the references to colour in this figure legend, the reader is referred to the Web version of this article.)

investigated the in vitro osteogenic differentiation of MC3T3-E1 cells on surfaces with different coatings. Following 7 days of osteogenic induction, ALP staining (Fig. 5a) and activity analysis (Fig. 5b) indicated enhanced early osteogenesis with Peptide-grafted coatings versus PC/Fe-MPNs. And the coatings supplemented with K₆-OGP (1:3, 2:2, 3:1, 0:4) was higher than that of the coatings grafted with K₆-RGD alone (4:0). PC/Fe@K₆-RGD/OGP_(1:3) exhibited higher ALP activity than PC/Fe-MPNs or single peptides, demonstrating the synergistic effect of RGD and OGP. ARS staining (Fig. 5a) and calcium quantification (Fig. 5c) of MC3T3-E1 cultured in osteogenic induction medium for 21 days also showed dipeptide (2:2, 1:3) co-modified surfaces enhanced mineralization versus single peptides or PC/Fe-MPNs. Therefore, the osteoinduction of different surfaces showed the dependence of K₆-OGP content; sufficient K₆-OGP content (not less than 50 %) was crucial to promote the osteogenic differentiation of MC3T3-E1. Cell osteogenic differentiation is a complex process. PC/Fe@K₆-RGD/OGP_(2:2) was selected for subsequent RT-qPCR experiments, considering the promotion of proliferation, adhesion, migration and osteogenesis as well as its application in vivo.

RT-qPCR was further employed to evaluate the expression of β -catenin and osteogenic-related genes (OCN, OPN, ON and Collagen I) in MC3T3-E1 cells cultured on different coating surfaces for 7 days (Fig. 5d–h). The results showed that PC/Fe@K₆-RGD/OGP_(2:2) significantly upregulated the mRNA levels of β -catenin, OCN, OPN, ON and Collagen I in surface-cultured MC3T3-E1 cells. These levels were markedly different from those on the PC/Fe-MPNs coating and the surfaces grafted single peptides. The findings suggest that the newly designed material effectively upregulates the expression of osteogenic-related genes in MC3T3-E1 cells, with OPN showing the most significant upregulation. Moreover, the high expression of β -catenin indicates that PC/Fe@K₆-RGD/OGP may promote osteogenesis by activating the Wnt/ β -catenin pathway. Numerous studies have indicated the close association between the Wnt/ β -catenin pathway and osteogenic differentiation of MC3T3-E1 cells. To elucidate the plausible involvement of the Wnt/ β -catenin pathway in the enhanced expression of osteogenic-related genes mediated by the novel biomaterials, we used β -catenin small interference RNA (siRNA) to selectively block the Wnt/ β -catenin signaling pathway in MC3T3-E1 cells cultured with different coatings

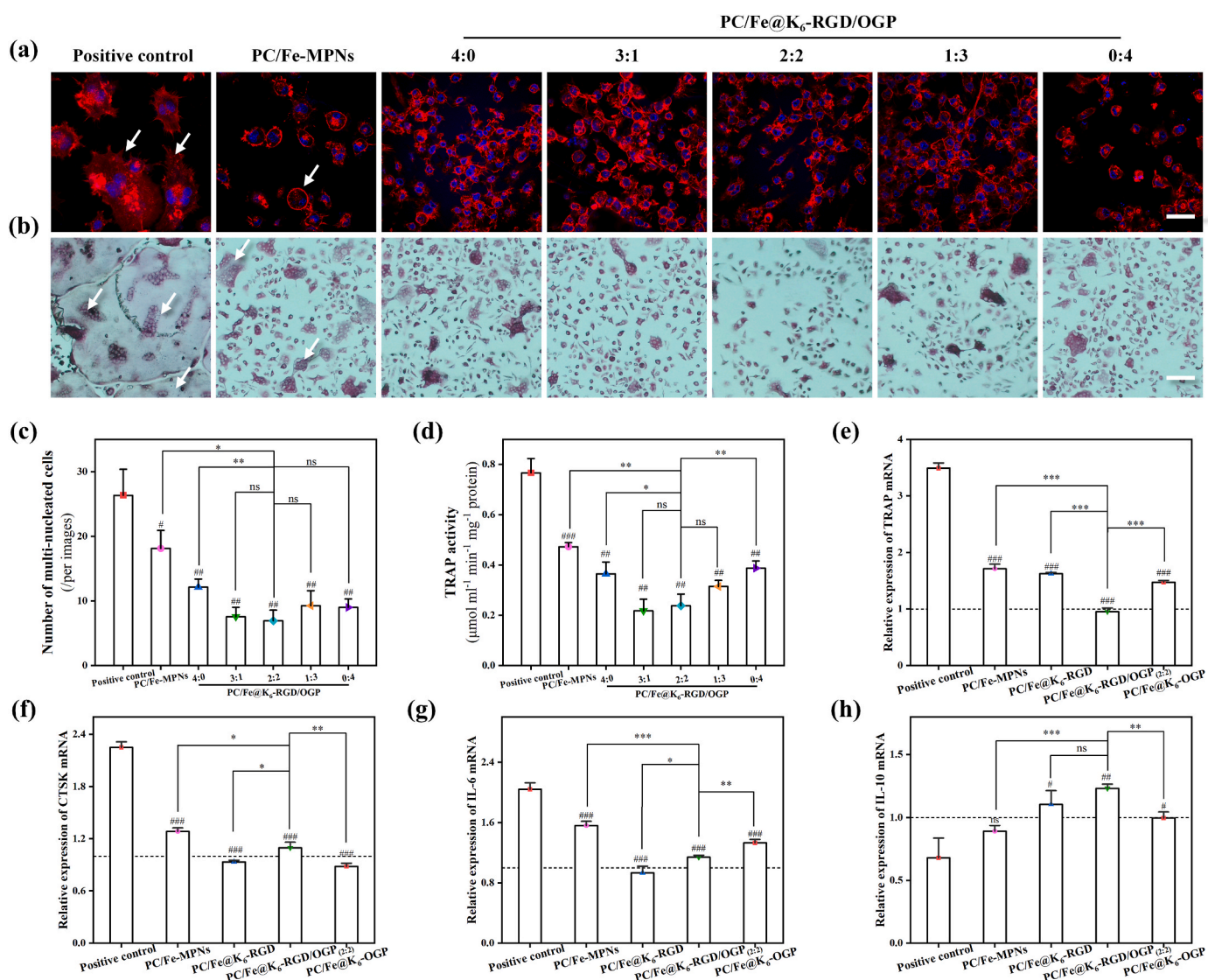


Fig. 6. Osteoclast differentiation of mBMMs on different modified substrates. (a) TRITC Phalloidin and (b) TRAP staining of mBMMs after 5 days of co-culture with different coatings in α -MEM medium containing 25 μ g/L M-CSF+50 μ g/L RANKL. (c) Multi-nucleated cell count analysis of (b). (d) Quantitative analysis of TRAP activity. Relative mRNA expression of (e) TRAP, (f) CTSK, (g) IL-6 and (h) IL-10 genes in mBMMs cultured on different modified substrates with different coatings in α -MEM medium containing 25 μ g/L M-CSF+50 μ g/L RANKL for 5 days. Scale bars in (a) are 50 μ m, scale bars in (b) are 200 μ m. (N \geq 3, no significance noted as "ns", *p < 0.05, **p < 0.01, ***p < 0.001 using *t*-test, and #p < 0.05, ##p < 0.01 or ###p < 0.001 compared with the Positive control group.)

for 7 days. Subsequently, we evaluated the mRNA expression of genes closely associated with osteogenesis. The study revealed that targeted silencing of β -catenin significantly impeded the upregulation of osteogenic-related genes in MC3T3-E1 cells cultured on the novel biomaterials (Fig. 5i–j). Therefore, it is plausible to propose that the PC/Fe@K₆-RGD/OGP_(2:2) coating enhances osteogenesis of MC3T3-E1 cells by inducing the activation of the Wnt/ β -catenin signaling pathway.

3.6. Anti-osteoclast differentiation of BMMs on different modified substrates

Bone remodeling relies on osteoclasts derived from the bone mononuclear macrophage lineage (BMM), so we investigated the effect of different coatings on mBMMs, focusing on their effect on osteoclastic differentiation. After 5 days, mBMMs treated with M-CSF and RANKL integrate to form multinucleated structures and grow substantially (Fig. 6a and b), while most mBMMs grown on coatings remained mononuclear morphology. Notably, PC/Fe-MPNs and PC/Fe@K₆-RGD/OGP coatings significantly reduced multinucleated cell formation, especially when the latter of RGD and OGP was grafted with peptide ratios of 2:2 (Fig. 6c). The TRAP activity assay showed a more than 3.5 times fold reduction in TRAP activity for mBMMs cultured on the PC/Fe@K₆-RGD/OGP_(2:2) coating compared to the control group (Fig. 6d). Moreover, this coating also significantly reduced TRAP activity compared to PC/Fe-MPNs and other single peptide grafted groups. Further, we assessed the expression levels of osteoclast differentiation and inflammatory genes in BMMs grown on PC/Fe@K₆-RGD/OGP_(2:2) and other coatings. All polyphenol-containing coatings significantly downregulated TRAP and CTSK gene expression compared with the control group (Fig. 6e and f). We also found a decrease in the pro-inflammatory marker IL-6 and an increase in the anti-inflammatory marker IL-10 in all cells cultured with polyphenol-containing coatings (Fig. 6g and h), and the changes in the PC/Fe@K₆-RGD/OGP_(2:2) coating group seemed to be the most definitive.

Excessive osteoclast activation on implant surfaces can lead to abnormal bone resorption and implantation failure, while appropriate osteoclast activity is critical for bone regeneration and remodeling. Previous studies have shown that polyphenols such as PC can inhibit osteoclast differentiation by modulating signaling pathways including RANKL-RANK [34] and NF- κ B [35], and OGP and RGD peptide also plays a regulatory role in osteoclast adhesion, proliferation and differentiation [36,37]. Our results demonstrated that the rationally designed PC/Fe@K₆-RGD/OGP_(2:2) coating retains these potentials, effectively controlling excessive osteoclast activation while preserving necessary osteoclast activity. And the RT-QPCR results suggested that the immune microenvironment might play a key role in the osteoclast differentiation on the coated surface.

3.7. Polarization of macrophage and antioxidant activity of MC3T3-E1 on different modified substrates

Macrophages, a class of white blood cells with critical immunological roles, can be polarized into distinct states (M0, M1, M2), each tasked with specific biological functions [38]. The status of macrophages plays a crucial role in the outcome following the implantation of biomaterials. In the presence of LPS and IFN- γ , all coated surfaces showed a significant reduction in the proportion of M1 phenotype macrophages (CD86⁺) compared to Ti surfaces (Fig. 7a–b). Interestingly, compared to other coatings, surfaces mainly grafted with K₆-RGD peptides (4:0, 3:1, 2:2) demonstrated a clearer inhibition of M1 macrophage polarization. Conversely, all coatings increased the proportion of M2 phenotype macrophages (CD206⁺) (Fig. 7a, c). Notably, surfaces grafted with K₆-OGP peptides (2:2, 1:3, 0:4) distinctly increased the proportion of M2 phenotype macrophages (CD206⁺) compared to PC/Fe-MPNs surfaces. Among these coatings, the PC/Fe@K₆-RGD/OGP_(2:2) coating retained the activity of PC and RGD in inhibiting M1 macrophage polarization

and the activity of OGP peptide in promoting M2 macrophage polarization, which was used for further study. M1 macrophages induce local inflammation by secreting TNF- α , IL-1 β , IL-6, IL-12, etc., while M2 macrophages secrete factors like IL-4, IL-10, VEGF, regulating angiogenesis, fibrosis and tissue repair processes. ELISA analysis of the cell culture supernatant revealed a significant decrease in the inflammatory factor (TNF- α) (Fig. 7d) and a substantial increase in the anti-inflammatory factor (IL-10) (Fig. 7e) and angiogenic (VEGF) (Fig. 7f) factors secreted by macrophages on the PC/Fe@K₆-RGD/OGP_(2:2) coating surface. The decrease in TNF- α , and increase in IL-10 are majorly attributed to the anti-inflammatory capacity of PC, while the increase of VEGF mainly depended on the pro-angiogenic ability of RGD peptide.

Subsequently, Ti plates modified with PC/Fe@K₆-RGD/OGP_(2:2) coating were implanted into rats for 5 days to observe their modulatory effect on macrophages (Fig. 7g). The polarization pattern induced by bare Ti substrates predominantly manifested as a significant increase in M1 macrophages, likely associated with a marked inflammatory response at the implantation site. Quantitative results revealed that PC/Fe@K₆-RGD/OGP coating significantly promoted a significant increase in M2 macrophages (Fig. 7h), suggesting an *in vivo* anti-inflammatory effect. Collectively, these results indicate that PC/Fe@K₆-RGD/OGP coating can provide a material-friendly microenvironment around the implant, promoting osteogenesis and osseointegration.

Under normal physiological conditions, ROS production and elimination are dynamically balanced. However, damage, implant insertion, or long-term implant wear can hardly avoid inducing a high-ROS environment [39]. Ideally, materials should be designed to lower intracellular ROS levels. In the presence of hydrogen peroxide, DCFH-DA green fluorescence intensity significantly increased in the positive control MC3T3-E1 cells, while cells co-cultured on different coatings did not show notable enhancement (Figs. S6a–c). This depended mainly on the anti-ROS capability of the PC/Fe-MPNs coating, which the newly designed PC/Fe@K₆-RGD/OGP coating well retained. ROS, arising as cell metabolism byproducts, act as second messengers intracellularly and participate in various biological processes as important regulatory factors balancing immune cells and bone/osteoclast homeostasis [40]. Excessive ROS levels have been shown to suppress osteoblast function and obstruct bone matrix secretion and mineralization [41]. Concurrently, ROS stress also activates osteoclasts via RANKL, inducing M1 macrophage polarization and bone resorption [42]. Thus, the superior anti-inflammatory and antioxidant properties of PC/Fe@K₆-RGD/OGP_(2:2) coating could counteract peri-implant inflammation and ROS stress, ultimately enhancing *in vitro* and *in vivo* osteogenesis [3].

3.8. Osteogenesis and osseointegration *in vivo*

The *in vitro* experiments demonstrated that composite coatings modulate multiple cell behaviors, with varied RGD: OGP peptide ratios promoting specific biological effects. This can be attributed to the complex interplay between RGD-integrin interactions and OGP signaling pathways. RGD facilitates cell adhesion, while OGP has osteoinductive and immunomodulatory properties [43,44]. Thus, the optimal ratio for particular cellular responses may differ. However, our results indicate a 2:2 RGD:OGP ratio has balanced impacts on cell adhesion, osteogenic differentiation, and inflammation inhibition, collectively benefiting overall bone repair *in vivo*. Therefore, to demonstrate the synergistic advantage of the dipeptide coating, we selected this ratio for the animal experiments.

Bone defect healing involves intricate coordinated processes with multiple interacting cell types *in vivo* [45]. While *in vitro* studies demonstrate isolated effects, *in vivo* assessments reflect cumulative osteogenic and osseointegrative impacts. To further validate the osteogenic and osseointegrative of the designed materials *in vivo*, we coated Ti rods with PC/Fe-MPNs and PC/Fe@K₆-RGD/OGP_(4:0, 2:2, 0:4) coatings and implanted them into rat femoral supracondylar bone defects

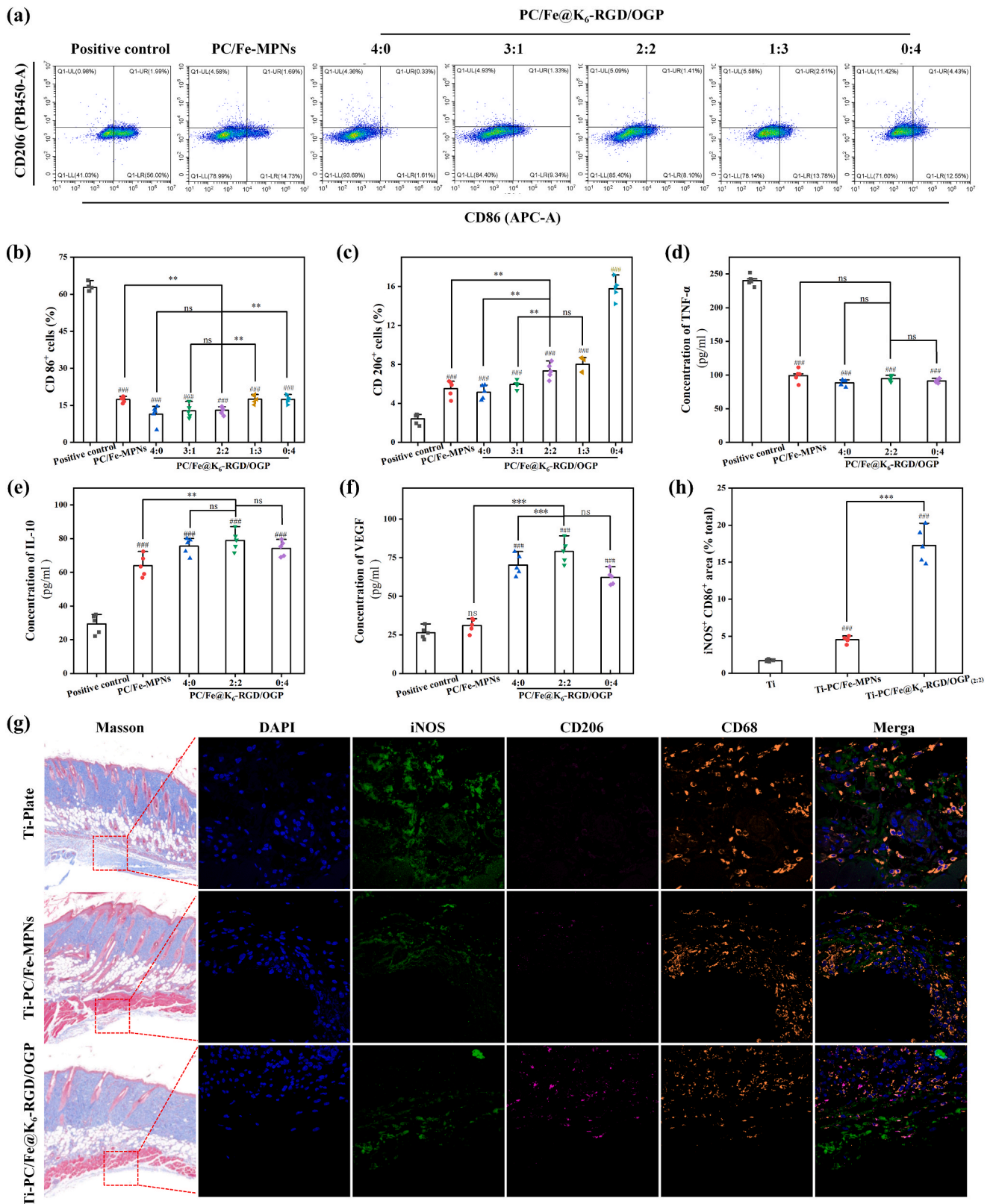


Fig. 7. Polarization of macrophage on different modified substrates. **(a)** Flow cytometric analysis demonstrating M1 (CD86⁺) and M2 (CD206⁺) phenotypic polarization of macrophages on various coatings. Quantitative analysis presents the proportion of M1 **(b)** and M2 **(c)** macrophages. Secreted **(d)** pro-inflammatory factors (TNF-α), **(e)** anti-inflammatory (IL-10), and **(f)** angiogenic (VEGF) factors by macrophages on distinct coating surfaces, respectively. **(g)** Immunofluorescence images showing different modified Ti substrates regulating macrophage polarization in the rats. **(h)** Quantitative analysis of the polarization of macrophages in vivo. Scale bars in **(g)** are 50 μm. (N ≥ 3, no significance noted as “ns”, *p < 0.05, **p < 0.01, ***p < 0.001 using t-test, and #p < 0.05, ##p < 0.01 or ###p < 0.001 compared with the Control group.)

(Fig. S7). By micro-CT scanning the removed femur together with the implants (Fig. 8a) and using CTvol software to reconstruct the 3D model, the formation of new bone around the implants in each group can be visually observed (Fig. 8b). Quantitative bone volume fraction (BV/TV) analysis revealed Ti-PC/Fe@K₆-RGD/OGP (2:2) implants generated substantially more new bone at 5 weeks compared to Ti-PC/Fe-MPNs and Ti-PC/Fe@K₆-OGP coatings (Fig. 8c). At 8 weeks, BV/TV of Ti-PC/Fe@K₆-RGD/OGP (2:2) implants was $13.68 \pm 0.756\%$, over 1.66 times fold that of uncoated Ti and significantly higher than other coatings. Trabecular number (Tb. N) followed a similar trend (Fig. 8d), with all coatings exceeding bare Ti at 8 weeks, and Ti-PC/Fe@K₆-RGD/OGP (2:2) showing most significant differences.

Histological staining can directly observe the morphology of new bone at the interface of the bone implant. As shown in Fig. 8e, Ti-PC/Fe@K₆-RGD/OGP (2:2) surface had the newest bone (stained with toluidine blue) and showed a mature lamellar bone structure. This group also had the largest contact area (red line frame) between the implant and the new bone and the implant, showing a significant osseointegration effect. On the other hand, the bare Ti and PC/Fe-MPNs showed less new bone formation, and the bone mineral deposits were scattered. Bone-implant contact (BIC) quantitatively confirmed enhanced osteointegration of Ti-PC/Fe@K₆-RGD/OGP (2:2), with BIC 3.06 times and 2.61 times fold of Ti at 5 and 8 weeks respectively, and significantly higher than single peptide coatings (Fig. 8f). This is consistent with the

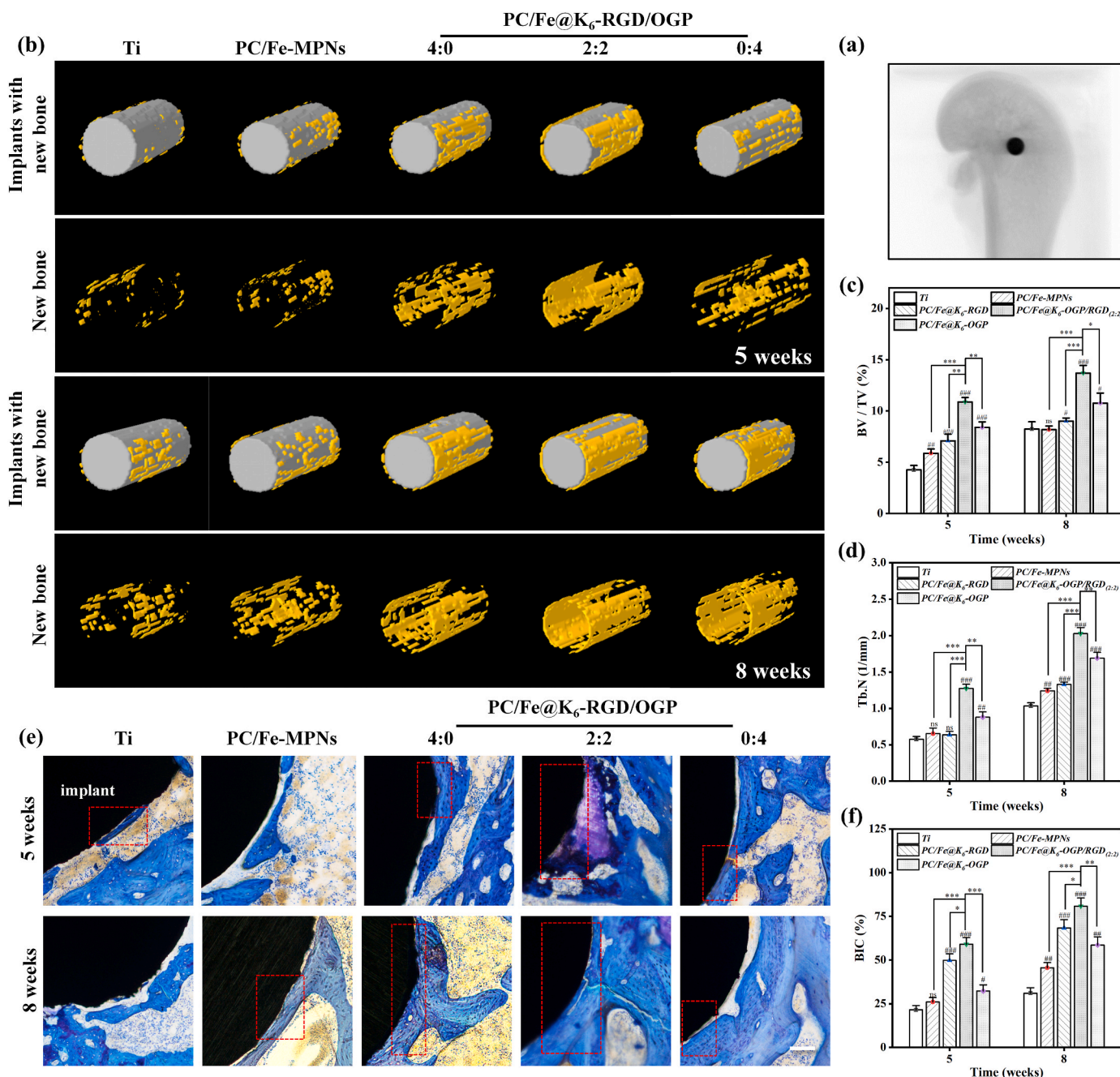


Fig. 8. Osteogenesis and osseointegration in vivo of PC/Fe@K₆-RGD/OGP. (a) Schematic diagram of micro-CT scanning. (b) Representative micro-CT 3D reconstructed images. (c) Quantitative analysis of peri-implant bone volume fraction (BV/TV). (d) Quantitative analysis of peri-implant trabecular bone number (Tb. N). (e) Representative histological images of different coated Ti rods stained with toluidine blue. (f) The average histomorphometric values of bone-implant contact (BIC). Scale bars in (e) are 100 μm . (N \geq 3, no significance noted as “ns”, *p < 0.05, **p < 0.01, ***p < 0.001 using t-test, and #p < 0.05, ##p < 0.01 or ###p < 0.001 compared with the Control group.). (For interpretation of the references to colour in this figure legend, the reader is referred to the Web version of this article.)

results of the pull-out mechanics test, and the Ti-PC/Fe@K₆-RGD/OGP (2:2) coating requires the highest pull-out force (Figs. S8a–d).

Notably, Ti-PC/Fe@K₆-RGD facilitated early osteointegration but had no impact on bone regeneration at 5 and 8 weeks. Ti-PC/Fe@K₆-OGP showed poor early osteointegration at 5 weeks but promoted bone formation throughout, especially at 8 weeks. Thus, RGD and OGP peptides synergistically regulate osteointegration and bone remodeling, with RGD dominant in early osteointegration and OGP in bone regeneration and reconstruction. Ti-PC/Fe@K₆-RGD/OGP (2:2) harnesses both advantages, demonstrating superior osteogenic and osseointegrative properties in vivo.

3.9. Stability and application of PC/Fe@K₆-RGD/OGP coating

A comprehensive evaluation of the in vivo stability and application prospects of the PC/Fe@K₆-RGD/OGP coating was conducted. In order to meet the needs of orthopedic implant coating materials, the selected materials need to be able to resist the digestion process in the body, and also need to maintain their effects for a long time after implantation in the body. First, the surface of bare Ti rods and Ti-PC/Fe@K₆-RGD/OGP-coated rods, which was gently removed from the decalcified femur, was observed using SEM. The results showed that the PC/Fe@K₆-RGD/OGP coating formed a uniform and complete coverage on the Ti rod surface before implantation (Fig. 9a). After 5 weeks and 8 weeks of

implantation, the surface structure of the coating was intact and maintained good uniformity, although a thinning trend of the coating thickness could be observed at high magnification. These results suggest that the Ti-PC/Fe@K₆-RGD/OGP coating may begin to decompose and degrade during long-term application, but overall maintain good stability.

Bone screws are one of the most promising types of orthopedic implants. Therefore, we further explored how the Ti-PC/Fe@K₆-RGD/OGP coating resisted shear wear during implantation into cortical bone (Fig. S9). The experimental results showed that the Ti-PC/Fe@K₆-RGD/OGP coating could completely and uniformly cover the surface of Ti screws before implantation (Fig. 9b). During the implantation process, the coating on the bottom of the thread and the sidewall of the thread still maintained uniformity (Fig. 9c), although the coating on the top of the thread of the Ti screw was partially peeled off due to the strong shear force generated by the screw torsion. These results indicate that the Ti-PC/Fe@K₆-RGD/OGP coating has anti-wear potential in this application scenario. These findings provide a preliminary understanding of the potential of Ti-PC/Fe@K₆-RGD/OGP coating for orthopedic implants. However, more studies on long-term stability and wear resistance are needed to better apply this coating clinically.

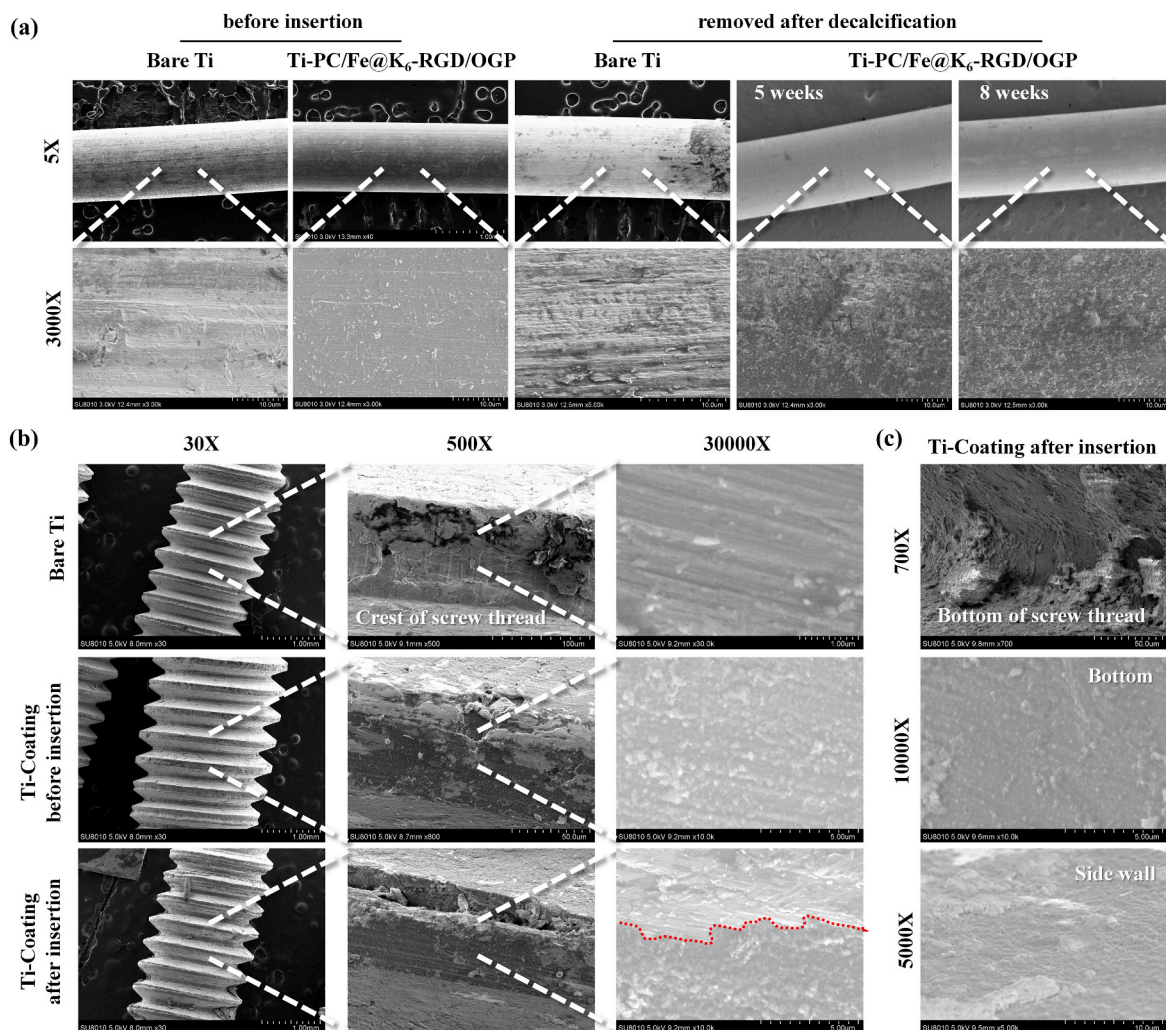


Fig. 9. Stability and application of Ti-PC/Fe@K₆-RGD/OGP coating. (a) SEM representative images of PC/Fe@K₆-RGD/OGP coated Ti rods before and after implantation in vivo. Representative SEM images of the (b) top and (c) bottom threads of the coated peptide bone screw before and after screw in and out at the diaphyseal site of the isolated bone.

4. Conclusions

In this study, we designed a biomimetic PC/Fe@K₆-RGD/OGP hybrid coating for orthopedic implants through a simple surface modification strategy. Co-immobilization of RGD and OGP peptides on the surface of MPNs by the K₆ group can precisely control the graft ratio and synergistically regulate osteogenesis. Importantly, the optimized PC/Fe@K₆-RGD/OGP coating demonstrated superior capacities for promoting MC3T3-E1 adhesion, proliferation, and osteogenic differentiation at specific RGD and OGP ratios. This hybrid coating also attenuated osteoclast formation and inhibited the polarization of pro-inflammatory M1 macrophages while promoted the polarization of M2 macrophages. It also reduced oxidative stress, providing a microenvironment favoring osteogenesis. In a rat femoral defect model, the PC/Fe@K₆-RGD/OGP coating significantly enhanced new bone formation and bone-implant integration compared to single peptide or non-peptide coatings. Mechanistically, RGD primarily modulated early osteointegration while OGP dominated bone regeneration, and MPNs intermediate layer mainly regulated immunity and anti-oxidative stress.

Collectively, these findings validate the PC/Fe@K₆-RGD/OGP hybrid coating as a promising strategy for synergistically regulating osteogenesis and osseointegration. The simplicity of this approach provides a highly translatable solution for clinical application. This study demonstrates the potential of rationally engineered peptide-polyphenol synergies for next-generation bioactive implant coatings.

Formatting of funding sources

This work was supported by Start-up Funding from Wenzhou Institute, University of Chinese Academy of Science (WIUCASQD2021032). Medical Health Science and Technology Project of Zhejiang Provincial Health Commission (2024KY144, 2023RC207), the Wenzhou Public Welfare Science and Technology Research Project (Y20210436), National Natural Science Foundation of China (82302698).

CRedit authorship contribution statement

Zeyu Shou: Conceptualization, Investigation, Visualization, Writing - original draft, Writing - review & editing. **Zhibiao Bai:** Formal analysis, Investigation, Methodology, Project administration. **Han Zhou:** Methodology, Validation, Writing - review & editing. **Yizhe Shen:** Data curation, Writing - original draft. **Xiaojing Huang:** Conceptualization, Supervision. **Hongming Meng:** Methodology, Writing - original draft. **Chenwei Xu:** Data curation. **Shaohao Wu:** Software, Visualization. **Na Li:** Funding acquisition, Project administration, Resources, Supervision, Validation, Visualization. **Chun Chen:** Conceptualization, Funding acquisition, Supervision, Validation, Visualization, Writing - review & editing.

Declaration of competing interest

The authors declare that they have no known competing financial interests or personal relationships that could have appeared to influence the work reported in this paper.

Data availability

The data that has been used is confidential.

Acknowledgements

none.

Appendix A. Supplementary data

Supplementary data to this article can be found online at <https://doi.org/10.1016/j.mtbio.2023.100921>.

References

- [1] G. Chandra, A. Pandey, Biodegradable bone implants in orthopedic applications: a review - ScienceDirect, Biocybern. Biomed. Eng. 40 (2020) 596–610.
- [2] K.T. Kim, M.Y. Eo, T.T.H. Nguyen, S.M. Kim, General review of titanium toxicity, Int. J. Implant Dent. 5 (2019) 1–12.
- [3] S. Yang, Y. Wang, S. Luo, C. Shan, Y. Geng, T. Zhang, S. Sheng, X. Zan, Building polyphenol and gelatin films as implant coating, evaluating from in vitro and in vivo performances, Colloids Surf. B Biointerfaces 181 (2019) 549–560, <https://doi.org/10.1016/j.colsurfb.2019.05.058>.
- [4] Y. Zhu, D. Zhou, X. Zan, Q. Ye, S. Sheng, Engineering the surfaces of orthopedic implants with osteogenesis and antioxidants to enhance bone formation in vitro and in vivo, Colloids Surf. B Biointerfaces 212 (2022), 112319, <https://doi.org/10.1016/j.colsurfb.2022.112319>.
- [5] G. Wang, Y. Zhu, X. Zan, M. Li, Endowing orthopedic implants' antibacterial, antioxidant, and osteogenesis properties through a composite coating of nano-hydroxyapatite, tannic acid, and lysozyme, Front. Bioeng. Biotechnol. 9 (2021), 718255, <https://doi.org/10.3389/fbioe.2021.718255>.
- [6] H. Zhou, L. Yang, U. Gbureck, S.B. Bhaduri, P. Sikder, Monetite, an important calcium phosphate compound-its synthesis, properties and applications in orthopedics, Acta Biomater. 127 (2021) 41–55, <https://doi.org/10.1016/j.actbio.2021.03.050>.
- [7] Z. Bai, K. Hu, Z. Shou, J. Yu, H. Meng, H. Zhou, L. Chen, T. Yu, R. Lu, N. Li, C. Chen, Layer-by-layer assembly of procyranidin and collagen promotes mesenchymal stem cell proliferation and osteogenic differentiation in vitro and in vivo, Regen. Biomater. 10 (2023), <https://doi.org/10.1093/rb/rbac107>.
- [8] L. Ou, Y. Lan, Z. Feng, L. Feng, J. Yang, Y. Liu, L. Bian, J. Tan, R. Lai, R. Guo, Functionalization of SF/HAP scaffold with GO-PEI-miRNA inhibitor complexes to enhance bone regeneration through activating transcription factor 4, Theranostics 9 (2019) 4525–4541, <https://doi.org/10.7150/thno.34676>.
- [9] Y. Han, R.P.M. Lafleur, J. Zhou, W. Xu, Z. Lin, J.J. Richardson, F. Caruso, Role of molecular interactions in supramolecular polypeptide-polyphenol networks for engineering functional materials, J. Am. Chem. Soc. 144 (2022) 12510–12519, <https://doi.org/10.1021/jacs.2c05052>.
- [10] C. Wang, Y. Liu, Y. Fan, X. Li, The use of bioactive peptides to modify materials for bone tissue repair, Regen. Biomater. 4 (2017) 191–206, <https://doi.org/10.1093/rb/rbx011>.
- [11] Q. Chen, X. Zhang, D. Zhang, G. Liu, K. Ma, J. Liu, K. Ma, M. Chen, Y. Li, R. Liu, Universal and one-step modification to render diverse materials bioactivation, J. Am. Chem. Soc. 145 (2023) 18084–18093, <https://doi.org/10.1021/jacs.3c05928>.
- [12] Z. Yuan, B. Tao, Y. He, J. Liu, C. Lin, X. Shen, Y. Ding, Y. Yu, C. Mu, P. Liu, K. Cai, Biocompatible MoS₂/PDA-RGD coating on titanium implant with antibacterial property via intrinsic ROS-independent oxidative stress and NIR irradiation, Biomaterials 217 (2019), 119290, <https://doi.org/10.1016/j.biomaterials.2019.119290>.
- [13] J. Bai, H. Wang, H. Chen, G. Ge, M. Wang, A. Gao, L. Tong, Y. Xu, H. Yang, G. Pan, P.K. Chu, D. Geng, Biomimetic osteogenic peptide with mussel adhesion and osteoimmunomodulatory functions to ameliorate interfacial osseointegration under chronic inflammation, Biomaterials 255 (2020), 120197, <https://doi.org/10.1016/j.biomaterials.2020.120197>.
- [14] T. Wang, J. Bai, M. Lu, C. Huang, D. Geng, G. Chen, L. Wang, J. Qi, W. Cui, L. Deng, Engineering immunomodulatory and osteoinductive implant surfaces via mussel adhesion-mediated ion coordination and molecular clicking, Nat. Commun. 13 (2022) 160, <https://doi.org/10.1038/s41467-021-27816-1>.
- [15] F. Gonzalez-Perez, A. Ibanez-Fonseca, M. Alonso, J.C. Rodriguez-Cabello, Combining tunable proteolytic sequences and a VEGF-mimetic peptide for the spatiotemporal control of angiogenesis within Elastin-Like Recombinamer scaffolds, Acta Biomater. 130 (2021) 149–160, <https://doi.org/10.1016/j.actbio.2021.06.005>.
- [16] K. Yu, J.C. Lo, Y. Mei, E.F. Haney, E. Siren, M.T. Kalathottukaren, R.E. Hancock, D. Lange, J.N. Kizhakkedathu, Toward infection-resistant surfaces: achieving high antimicrobial peptide potency by modulating the functionality of polymer brush and peptide, ACS Appl. Mater. Interfaces 7 (2015) 28591–28605, <https://doi.org/10.1021/acsami.5b10074>.
- [17] L. Padiolleau, C. Chanseau, S. Durrieu, P. Chevallier, G. Laroche, M.C. Durrieu, Single or mixed tethered peptides to promote hMSC differentiation toward osteoblastic lineage, ACS Appl. Bio Mater. 1 (2018) 1800–1809, <https://doi.org/10.1021/acsabm.8b00236>.
- [18] J. Sun, Y. Huang, H. Zhao, J. Niu, X. Ling, C. Zhu, L. Wang, H. Yang, Z. Yang, G. Pan, Q. Shi, Bio-clickable mussel-inspired peptides improve titanium-based material osseointegration synergistically with immunopolarization-regulation, Bioact. Mater. 9 (2022) 1–14, <https://doi.org/10.1016/j.bioactmat.2021.10.003>.
- [19] M. Li, J. Bai, H. Tao, L. Hao, W. Yin, X. Ren, A. Gao, N. Li, M. Wang, S. Fang, Y. Xu, L. Chen, H. Yang, H. Wang, G. Pan, D. Geng, Rational integration of defense and repair synergy on PEEK osteoimplants via biomimetic peptide clicking strategy, Bioact. Mater. 8 (2022) 309–324, <https://doi.org/10.1016/j.bioactmat.2021.07.002>.
- [20] B. Zhao, Y. Dong, X. Shen, W. He, H. Jin, Y. Lili, S.w. Zheng, X. Zan, J. Liu, Construction of multifunctional coating with cationic amino acid-coupled peptides for osseointegration of implants, Mater. Today Bio 23 (2023), 100848, <https://doi.org/10.1016/j.mtbio.2023.100848>.

- [21] K.S. Rappe, M. Ortiz-Hernandez, M. Punset, M. Molmeneu, A. Barba, C. Mas-Moruno, J. Guillem-Marti, C. Caparros, E. Ruperez, J. Calero, M.C. Manzanares, J. Gil, J. Franch, On-growth and in-growth osseointegration enhancement in PM porous Ti-scaffolds by two different bioactivation strategies: alkali thermochemical treatment and RGD peptide coating, *Int. J. Mol. Sci.* 23 (2022), <https://doi.org/10.3390/ijms23031750>.
- [22] X. Li, Z. Liu, S. Xu, X. Ma, Z. Zhao, H. Hu, J. Deng, C. Peng, Y. Wang, S. Ma, A drug delivery system constructed by a fusion peptide capturing exosomes targets to titanium implants accurately resulting the enhancement of osseointegration peri-implant, *Biomater. Res.* 26 (2022) 89, <https://doi.org/10.1186/s40824-022-00331-0>.
- [23] J. Li, J. Wei, A. Li, H. Liu, J. Sun, H. Qiao, A dual peptide sustained-release system based on nanohydroxyapatite/polyamide 66 scaffold for synergistic-enhancing diabetic rats' fracture healing in osteogenesis and angiogenesis, *Front. Bioeng. Biotechnol.* 9 (2021), 657699, <https://doi.org/10.3389/fbioe.2021.657699>.
- [24] F.M. Costa, S.R. Maia, P.A. Gomes, M.C. Martins, Dhvar5 antimicrobial peptide (AMP) chemoselective covalent immobilization results on higher antiadherence effect than simple physical adsorption, *Biomaterials* 52 (2015) 531–538, <https://doi.org/10.1016/j.biomaterials.2015.02.049>.
- [25] K.-f. Ren, M. Hu, H. Zhang, B.-c. Li, W.-x. Lei, J.-y. Chen, H. Chang, L.-m. Wang, J. Ji, Layer-by-layer assembly as a robust method to construct extracellular matrix mimic surfaces to modulate cell behavior, *Prog. Polym. Sci.* 92 (2019) 1–34, <https://doi.org/10.1016/j.progpolymsci.2019.02.004>.
- [26] R. Lu, X. Zhang, X. Cheng, Y. Zhang, X. Zan, L. Zhang, Medical applications based on supramolecular self-assembled materials from tannic acid, *Front. Chem.* 8 (2020), 583484, <https://doi.org/10.3389/fchem.2020.583484>.
- [27] X. Cheng, Y. Zhu, S. Tang, R. Lu, X. Zhang, N. Li, X. Zan, Material priority engineered metal-polyphenol networks: mechanism and platform for multifunctionalities, *J. Nanobiotechnol.* 20 (2022) 255, <https://doi.org/10.1186/s12951-022-01438-1>.
- [28] N. Li, Z. Shou, S. Yang, X. Cheng, C. Chen, S. Zheng, Y. Shi, H. Tang, Subtle distinction in molecular structure of flavonoids leads to vastly different coating efficiency and mechanism of metal-polyphenol networks with excellent antioxidant activities, *Colloids Surf. B Biointerfaces* 229 (2023), 113454, <https://doi.org/10.1016/j.colsurfb.2023.113454>.
- [29] X. Cheng, R. Lu, X. Zhang, Y. Zhu, S. Wei, Y. Zhang, X. Zan, W. Geng, L. Zhang, Silanization of a metal-polyphenol coating onto diverse substrates as a strategy for controllable wettability with enhanced performance to resist acid corrosion, *Langmuir* 37 (2021) 3637–3647, <https://doi.org/10.1021/acs.langmuir.0c03623>.
- [30] R. Lu, B. Zhao, L. Yang, S. Zheng, X. Zan, N. Li, Role of driving force on engineering layer-by-layer protein/polyphenol coating with flexible structures and properties, *ACS Appl. Mater. Interfaces* 15 (2023) 20551–20562, <https://doi.org/10.1021/acsmi.3c02047>.
- [31] A.A. Al-Bari, A. Al Mamun, Current advances in regulation of bone homeostasis, *FASEB Bioadv.* 2 (2020) 668–679, <https://doi.org/10.1096/fba.2020-00058>.
- [32] Y. He, C. Mu, X. Shen, Z. Yuan, J. Liu, W. Chen, C. Lin, B. Tao, B. Liu, K. Cai, Peptide LL-37 coating on micro-structured titanium implants to facilitate bone formation in vivo via mesenchymal stem cell recruitment, *Acta Biomater.* 80 (2018) 412–424, <https://doi.org/10.1016/j.actbio.2018.09.036>.
- [33] W. Chen, K. Xu, B. Tao, L. Dai, Y. Yu, C. Mu, X. Shen, Y. Hu, Y. He, K. Cai, Multilayered coating of titanium implants promotes coupled osteogenesis and angiogenesis in vitro and in vivo, *Acta Biomater.* 74 (2018) 489–504, <https://doi.org/10.1016/j.actbio.2018.04.043>.
- [34] S. Tanabe, J. Santos, V.D. La, A.B. Howell, D. Grenier, A-type cranberry proanthocyanidins inhibit the RANKL-dependent differentiation and function of human osteoclasts, *Molecules* 16 (2011) 2365–2374, <https://doi.org/10.3390/molecules16032365>.
- [35] W. Zhu, Z. Yin, Q. Zhang, S. Guo, Y. Shen, T. Liu, B. Liu, L. Wan, S. Li, X. Chen, Z. Ouyang, D. Peng, Proanthocyanidins inhibit osteoclast formation and function by inhibiting the NF-kappaB and JNK signaling pathways during osteoporosis treatment, *Biochem. Biophys. Res. Commun.* 509 (2019) 294–300, <https://doi.org/10.1016/j.bbrc.2018.12.125>.
- [36] S. Ma, S. Xu, M. Li, Y. Du, G. Tian, J. Deng, W. Zhang, P. Wei, B. Zhao, X. Zhang, Z. Liu, Y. Wang, A bone targeting nanoparticle loaded ogp to restore bone homeostasis for osteoporosis therapy, *Adv. Healthcare Mater.* (2023), e2300560, <https://doi.org/10.1002/adhm.202300560>.
- [37] D. de Melo Pereira, N. Davison, P. Habibovic, Human osteoclast formation and resorptive function on biomaterialized collagen, *Bioact. Mater.* 8 (2022) 241–252, <https://doi.org/10.1016/j.bioactmat.2021.06.036>.
- [38] Q. Gu, H. Yang, Q. Shi, Macrophages and bone inflammation, *J. Orthop. Translat.* 10 (2017) 86–93, <https://doi.org/10.1016/j.jot.2017.05.002>.
- [39] S. Yang, Y. Wang, X. Wu, S. Sheng, T. Wang, X. Zan, Multifunctional tannic acid (TA) and lysozyme (lys) films built layer by layer for potential application on implant coating, *ACS Biomater. Sci. Eng.* 5 (2019) 3582–3594, <https://doi.org/10.1021/acsbomaterials.9b00717>.
- [40] H. Tao, G. Ge, X. Liang, W. Zhang, H. Sun, M. Li, D. Geng, ROS signaling cascades: dual regulations for osteoclast and osteoblast, *Acta Biochim. Biophys. Sin.* 52 (2020) 1055–1062, <https://doi.org/10.1093/abbs/gmaa098>.
- [41] M. Almeida, L. Han, M. Martin-Millan, C.A. O'Brien, S.C. Manolagas, Oxidative stress antagonizes Wnt signaling in osteoblast precursors by diverting beta-catenin from T cell factor- to forkhead box O-mediated transcription, *J. Biol. Chem.* 282 (2007) 27298–27305, <https://doi.org/10.1074/jbc.M702811200>.
- [42] H.Y. Tan, N. Wang, S. Li, M. Hong, X. Wang, Y. Feng, The reactive oxygen species in macrophage polarization: reflecting its dual role in progression and treatment of human diseases, *Oxid. Med. Cell. Longev.* 2016 (2016), 2795090, <https://doi.org/10.1155/2016/2795090>.
- [43] J. Liu, Y. Tang, W. Yang, B. Tao, Y. He, X. Shen, T. Shen, C. Lin, K. Cai, Functionalization of titanium substrate with multifunctional peptide OGP-NAC for the regulation of osteoimmunology, *Biomater. Sci.* 7 (2019) 1463–1476, <https://doi.org/10.1039/c8bm01611a>.
- [44] M. Yakufu, Z. Wang, Y. Wang, Z. Jiao, M. Guo, J. Liu, P. Zhang, Covalently functionalized poly(etheretherketone) implants with osteogenic growth peptide (OGP) to improve osteogenesis activity, *RSC Adv.* 10 (2020) 9777–9785, <https://doi.org/10.1039/d0ra00103a>.
- [45] S. Wei, J.X. Ma, L. Xu, X.S. Gu, X.L. Ma, Biodegradable materials for bone defect repair, *Mil. Med. Res.* 7 (2020) 54, <https://doi.org/10.1186/s40779-020-00280-6>.